HHS Public Access

Author manuscript

J Med Chem. Author manuscript; available in PMC 2018 November 09.

Published in final edited form as:

J Med Chem. 2017 November 09; 60(21): 8906–8922. doi:10.1021/acs.jmedchem.7b01154.

Small-Molecule Inhibitors of the CD40–CD40L Costimulatory Protein-Protein Interaction

Jinshui Chen[1,4], **Yun Song**[1,2,4], **Damir Bojadzic**[1], **Alejandro Tamayo-Garcia**[1], **Ana Marie Landin**[3], **Bonnie B. Blomberg**[3], and **Peter Buchwald**[1,2,*]

[1]Diabetes Research Institute, Miller School of Medicine, University of Miami, Miami, Florida 33136, USA

[2]Molecular and Cellular Pharmacology, Miller School of Medicine, University of Miami, Miami, Florida 33136, USA

[3]Microbiology and Immunology, Miller School of Medicine, University of Miami, Miami, Florida 33136, USA

Abstract

Costimulatory interactions are required for T cell activation and development of an effective immune response; hence, they are valuable therapeutic targets for immunomodulation. However, they, as all other protein-protein interactions, are difficult to target by small molecules. Here, we report the identification of novel small-molecule inhibitors of the CD40–CD40L interaction designed starting from the chemical space of organic dyes. For the most promising compounds such as DRI-C21045, activity (IC_{50}) in the low micromolar range has been confirmed in cell assays including inhibition of CD40L-induced activation in NF-κB sensor cells, THP-1 myeloid cells, and primary human B cells as well as in murine allogeneic skin transplant and alloantigen-induced T cell expansion in draining lymph node experiments. Specificity versus other TNF-superfamily interactions (TNF-R1–TNF-α) and lack of cytotoxicity have also been confirmed at these concentrations. These novel compounds provide proof-of-principle evidence for the

*Corresponding Author. Phone: 305 243-9657, pbuchwald@med.miami.edu, Diabetes Research Institute, Miller School of Medicine, University of Miami, 1450 NW 10 Ave, (R-134), Miami, FL 33136, USA.

[4]These authors contributed equally to the present work.

ASSOCIATED CONTENT

Supporting Information

The Supporting Information is available free of charge on the ACS Publications website at DOI: …

Figure S1–S7 and Scheme S1–S3: Inhibition of the Mac-1–CD40L interaction; Inhibition of CD40L-induced MHC-II upregulation in THP-1 cells; MTT cytotoxicity assessment in THP-1 cells; mutagenicity assessment (Ames test); inhibition of CD40L-induced human B cell proliferation; flow cytometry histograms illustrating the inhibition of CD40L-induced human B-cell function (AID activation); CD40–CD40L blocking activity of KGYY15 15-mer CD40 peptide inhibitors; and syntheses of compounds **5**, **7**, and **11** (PDF).

Molecular formula strings (CSV)

Author contributions

J.C. performed all chemical synthesis and contributed to the design of new structures, Y.S. performed the majority of the experiments; D.B. performed some screening assays, the draining lymph node assay, the Ames test, and helped with some of the mice experiments; A.T.G. performed the mice experiments; A.M.L. performed the B cell activity assays; B.B. provided study guidance for the immune experiments and suggested the B cell activity assay; P.B. originated and designed the project, provided study guidance, and wrote the bulk of the manuscript. All authors read and revised the manuscript.

Competing financial interest

The University of Miami has filed a patent on these compounds with Peter Buchwald as inventor. All other authors declare no competing financial interests.

possibility of small-molecule inhibition of costimulatory protein-protein interactions, establish the structural requirements needed for efficient CD40–CD40L inhibition, and serve to guide the search for such immune therapeutics.

TABLE OF CONTENTS GRAPHIC

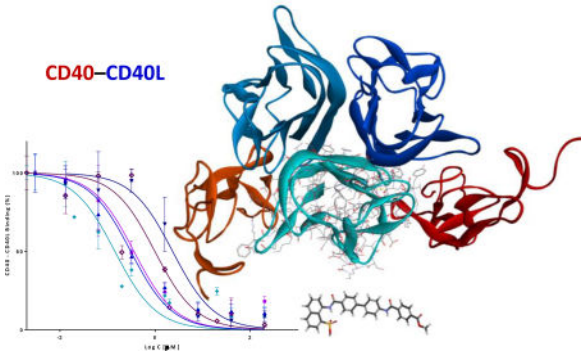

INTRODUCTION

It is now well-recognized that co-stimulatory and co-inhibitory signaling play crucial roles in the activation of immune responses and in T cell biology as they determine the functional outcome of T cell receptor (TCR) signaling[1]. In addition to the engagement of the TCR by the MHC-peptide complex, T cell activation also requires the ligation of costimulatory molecules on T cells with their respective ligands on antigen-presenting cells (APCs). If this second signal is lacking, T cells will not be activated and will not undergo proliferation, cytokine production, or further differentiation into effector cells. While the underlying mechanisms are not entirely understood, it is generally believed that antigen recognition (TCR) in the absence of costimulation can alter the immune response and lead to tolerance. Consequently, costimulatory modulation could provide immunomodulatory (IM) agents that are activation-and antigen-specific, thus, safer and more effective than existing IM therapies. Costimulatory interactions have emerged as particularly valuable therapeutic targets in transplant recipients and in autoimmune diseases for exactly these reasons[2–8]. They are cell surface protein-protein interactions (PPIs) that belong to two main families: the immunoglobulin superfamily (e.g., CD28/CTLA4–CD80/86 and ICOS–ICOS-L) and the TNF–TNFR superfamily (TNFSF).

Among TNFSF interactions, we are particularly interested in the blockade of the CD40–CD40L interaction (Figure 1)[9, 10] because this seems to be particularly effective in islet transplantations[11, 12]. This pathway is also a promising target in a number of autoimmune diseases[7, 13–15], including type 1 diabetes (T1D)[16–19]. In fact, CD40 (TNFRSF5) and CD40L (CD154, TNFSF5) were the first TNFSF costimulatory molecules identified[6], and this PPI is among the most extensively studied TNFSF members. CD40 is a transmembrane glycoprotein constitutively expressed on APCs, whereas its ligand, CD40L, exists both as a transmembrane protein and a soluble form in the plasma[20–22]. The interaction between CD40L on T cells and its receptor CD40 on B cells is essential for lymphocyte signaling leading to T cell-dependent B cell proliferation, immunoglobulin class switching, and B-cell

maturation. Mutations of CD40L expressed on T cells are known to result in X-linked hyper-IgM syndrome (XHIGM), a primary immunodeficiency characterized by an inability to produce immunoglobulins of IgG, IgA, and IgE isotypes[23], indicating the important role of CD40–CD40L in CSR (class switch recombination). In addition to the role played by the CD40–CD40L interaction in immune responses[7], there is increasing evidence for its role in atherosclerosis, cardiovascular disease, acute coronary syndrome, thrombosis, inflammation, inflammatory bowel disease, and even metabolic syndrome[24–26]. Intriguingly, recent evidence also indicates that the CD40–CD40L interaction plays an important role in glucolipotoxicity-induced β-cell death[27].

Consequently, inhibition of CD40 signaling can be beneficial in the pathogenic processes of chronic inflammatory diseases, such as autoimmune diseases, neurodegenerative disorders, graft-versus-host disease, cancer, and atherosclerosis[8]. Multiple antibodies targeting this interaction have been developed and are in preclinical or clinical development – for example, bleselumab, lucatumumab, dacetuzumab, and others[8]. Clinical trials of ruplizumab (hu5c8), an anti-CD40L humanized antibody, looked promising; however, they have been halted because of possible thrombolytic side effects[28–31], and development is no longer supported[32]. Activated platelets express CD40L; however in platelet-rich plasma, the 5c8 antibody by itself did not induce platelet aggregation *per se* and did not significantly affect maximal aggregation. This side effect may be partly due to the antibody nature of the therapy, and a pro-aggregation effect of the antibody by a mechanism involving the mAb Fc domain has been suggested[33]. Along these lines, more recently developed so-called Fc-silent domain antibodies (dAbs) that do not bind to FcgRIIa, including letolizumab, were found to retain immunomodulatory activity, but do not activate platelets[34, 35].

Antibodies (immunoglobulins) can be highly specific for their targets and quite stable in human serum; however, being protein therapeutics, their development is often hindered by the possibility of a strong immune response mounted against them[36]. Even among novel therapeutics approved by the FDA, post-market safety events were found to be significantly more frequent among biologics[37]. Development of IM biologics is further complicated by the high likelihood of unwanted adverse reactions that include serious infections, malignancy, cytokine release syndrome, anaphylaxis, hypersensitivity, and immunogenicity[38]. Out of 40 licensed IM biologics, 18 have been associated with serious infections, including reactivation of bacterial, viral, fungal, and opportunistic infections[38]. Peptide inhibitors have been explored as possible alternatives. For example, a CD40–CD40L blocking cyclic heptapetide (CLPTRHMAC) has been shown not to prime human platelet activation and aggregation in *in vitro* platelet activation studies, contrary to the anti-CD40L mAb also tested[39]. More recently, a CD40-targeting peptide (VLQWAKKGYYTMKSN designated as mouse $KGYY_{15}$), which was designed from the CD40L domain critical for interaction with CD40, has been shown to be effective in preventing T1D in NOD (non-obese diabetic) mice, a well-known animal model of this disease[19]. In addition to CD40, CD40L also binds to integrins, such as $\alpha_{IIb}\beta_3$ and Mac-1 ($\alpha_M\beta_2$), mediating different inflammatory pathologies including atherosclerosis, and these interactions could also be blocked by peptide inhibitors[40, 41]. However, peptides, just as antibodies, are unlikely to be formulated for oral administration, which is an important consideration for prospective T1D preventive therapies that have to be sufficiently patient friendly[42] (to allow the long-term

adherence and compliance needed for a successful preventive therapy). An IM therapy that could prevent or revert recent-onset T1D is of particular interest as all existing IM therapies tested to date in large-scale human clinical trials have failed to stop the progressive decline of the function of insulin-producing pancreatic β-cells[43–48]. Even the most successful immunological interventions (e.g., cyclosporine, teplizumab, otelixizumab, rituximab, and abatacept) achieved no more than a few months delay in the decline of insulin production, and prevention with parenteral insulin or GAD-vaccine did no better[43, 48]. Currently, T1D is one of the few remaining autoimmune diseases without any approved immunological treatment[49].

We decided, therefore, to focus on identifying small-molecule compounds that can interfere with the CD40–CD40L costimulatory PPI. However, PPI inhibition with small-molecule compounds is challenging and, for a long time, has been considered unlikely to be successful. PPIs usually involve relatively large protein surfaces (1,500–3,000 $Å^2$)[50, 51] and lack the well-defined binding pockets present on traditional targets of most existing drugs, such as G-protein coupled receptors, ion channels, and enzymes, making it difficult for small molecules to bind with high enough energy / affinity. Within the last few years, however, sufficiently effective small-molecule inhibitors have been identified for several important PPIs, and there are now >40 PPIs targeted by small molecules that are in preclinical development[51–63]. Venetoclax, which was identified from a small-molecule series designed to target PPIs in the B cell lymphoma 2 (BCL-2) family[64], has just received FDA approval for clinical use[65]. Lifitegrast, a small molecule LFA-1–ICAM-1 inhibitor[66], has also been approved recently by the FDA for the treatment of dry eye[63]. Focusing on the CD40–CD40L PPI, we have first identified suramin as a small-molecule inhibitor with a half-maximal inhibitory concentration (IC_{50}) in the 50 μM range[67] and then a set of organic dyes such as those illustrated by structures **1**–**4** (Figure 2) that concentration-dependently inhibited this costimulatory PPI with activities in the low micromolar range[68, 69]. Among organic dyes, we have also identified small-molecule inhibitors of the OX40–OX40L costimulatory PPI[70] as well as the first promiscuous small-molecule PPI inhibitor[71, 72]. Here, we present a set of new and more potent small-molecule inhibitors of the CD40–CD40L interaction (**5**–**11**) that were designed starting from the chemical space of these organic dyes (**1**–**4**, Figure 2), but are more drug-like and no longer contain color-causing chromophores.

RESULTS

Design

To identify novel small-molecule compounds that can inhibit the CD40–CD40L costimulatory protein-protein interaction (PPI) (Figure 1), we started from our previously identified organic dye inhibitors such as **1** or **4** (Figure 2)[68, 69] and synthesized new chemical entities that maintain the main molecular framework, but lack the aromatic azo chromophores responsible for their vivid color. Compounds explored here (**5**–**11**, Figure 3) maintain the aromatic ring scaffold, but the azo linkers are replaced with amide ones. We used an iterative design, synthesis, testing, and redesign approach, and found that several structural elements need to be maintained for activity. We originally started with structures with a single ring linker (such as in **5**, Figure 3), but found that use of a two ring linker (such

as in **6**) significantly improved activity as illustrated by the three orders of magnitude improvement in IC_{50}s (0.3 vs. 342 μM for **6** vs. **5**, Table 1). All explored structures lacking a naphthalene ring or polar substitutions on both terminal aromatic rings (R_1, R_2) also showed considerably diminished activity. Hence, structures tested here all have two-ring linkers (i.e., **6** – **11**, Figure 3).

Synthesis

All new compounds were synthesized following a similar route that involved a general procedure of amide coupling (Scheme 1). The synthesis of compound **6** (DRI-C21041)[73] is shown for illustration. It involved three steps consisting of two amide couplings (using a modified version of the procedure of Venkatraj and co-workers[74]) and one hydrogenation (using a modified version of the procedure of Kassack and co-workers[75]) (Scheme 1). The first amide coupling of the commercially available amine **12** and acid **13** gave the nitro derivative **14**. The following hydrogenation provided the amine derivative **15**. The second amide coupling of the amine **15** and the acid **16** furnished the final product **6** (total yield 49%). The synthesis of most other compounds was achieved via the same three steps using the biphenyl as an aromatic linker in the first step (*a*) and different acids as coupling partners in the third step (*c*). Compound **8** (DRI-C21042)[73] was simply synthesized in one step by hydrogenation of **6**. Compounds **7** and **11** were assembled using the corresponding differently substituted naphthyl rings. Details are summarized in the experimental section.

Binding Inhibition

CD40–CD40L—The ability of compounds **5**–**11** (Figure 3; Table 1) to inhibit the CD40–CD40L interaction was quantified using a cell-free *in vitro* binding inhibition assay measuring the amount of soluble CD40L (CD154) bound to plate-coated CD40 in the presence of increasing concentrations of test compounds as described before[67, 68]. Organic dye **1** from our previous work was used as reference control. As the binding inhibition data show (Figure 4A), compounds **6**, **7**, **9**–**11** concentration-dependently inhibited the CD40–CD40L interaction in this assay with activities in the high nanomolar to low micromolar range as indicated by the corresponding IC_{50} values. In general, concentration-dependencies were adequately described by a standard log inhibitor vs. response model (i.e., a classical sigmoid binding function with a Hill slope of 1). All IC_{50} values shown in Table 1 were obtained by fitting this model. Compounds **6**, **10** (DRI-C21045), and **11** (DRI-C25441)[73] showed particularly promising activities with IC_{50} values of 0.31, 0.17, and 0.36 μM, respectively – about an order of magnitude better than our reference dye compound **1** (direct red 80). Meanwhile, compounds **5**, with a single ring linker, and **8**, with an amine substituent, showed very little activity (IC_{50} > 300 μM) – clear evidence of structural selectivity at the binding site (see Discussion). Because polymolecular conglomeration[76, 77] / aggregation[78, 79] is a frequent cause of promiscuous inhibition in screening assays[80], we have checked for this by adding a non-ionic detergent (Triton-X 100, 0.01%) to the binding inhibitory assay, as recommended for the detection of such effects[81]. This already has been shown to have no effect for our original leads[68], not even for the promiscuous PPI inhibitor erythrosine B (ErB)[71]. We have rechecked again here for the present compounds, and the presence of the detergent caused slight, but no significant shifts

in the IC_{50}s of all compounds, e.g., **10** (1.2×), **11** (1.9×), or ErB (1.04×) with the exception of **6**, our least soluble compound, which was more strongly shifted (8.0×). An illustrative example is included in Supporting Information Figure S7.

Selectivity/specificity—In addition to adequate activity, sufficient selectivity and specificity are also desirable. Typically, small-molecule compounds are considered to be promising enough leads if they show 30–100-fold selectivity over other possible pharmacological targets of interest[82, 83]. To check for this, we assessed the ability of these compounds to inhibit the TNF-R1–TNF-α interaction, which is part of the same TNF superfamily receptor-ligand interaction (Figure 4B). All active new compounds showed >100 fold selectivity in their ability to inhibit the CD40 vs. the TNF interaction (Table 1), which further supports structural specificity and argues against a possible promiscuous (e.g., aggregation-related) effect. Because in addition to its CD40 receptor, CD40L also binds to integrins such as Mac-1 ($\alpha_M\beta_2$)[41], we tested the ability of the present compounds to inhibit this interaction using a similar assay. Most of the tested compounds showed similar activity (Supporting Information Figure S1) with the dye control **1** and the amine **8** showing about 10-fold increased inhibitory potency.

In Vitro Activity

Inhibition of CD40L-induced NF-κB activation—To confirm the activity of our compounds in a cell-based model, we used sensor cells containing a secreted embryonic alkaline phosphatase (SEAP) reporter gene under the control of a promoter fused to an NF-κB binding site and transfected with CD40. In these cells (HEK Blue CD40) the secretion of SEAP is specifically induced by the binding CD40L to its cell-surface receptor (CD40) and the downstream activation of the corresponding NF-κB pathway. A monoclonal anti-CD40L antibody was used as a positive control. All tested compounds (**1** as well as **6**, **10**, and **11**) showed concentration-dependent inhibition of the activation of NF-κB in these cells that was induced by CD40L as shown in Figure 5 with activities in the low micromolar range (Table 1). For all compounds (including the reference compound **1**), the corresponding IC_{50}s are about an order of magnitude higher than those determined in the cell-free binding inhibition assay (Table 1), a loss of activity most likely due to the presence of proteins and cells in this assay causing some loss by non-specific binding.

Inhibition of CD40L-induced marker expression in THP cells—CD40L also induces various responses in dendritic cells, human myeloid THP-1 cells, and other human acute myeloid leukemia (AML) cells. These responses include, for example, morphological changes, cell proliferation, rescue from apoptosis, secretion of IL-2 and other cytokines, as well as the up-regulation of the expression of adhesion and costimulatory molecules such as CD54, CD86, CD80, MHC-II, and CD40 itself[84]. As before[68], as an additional *in vitro* cell assay to assess the inhibitory potential of the present compounds, we quantified their effect on the expression of CD40L-induced MHC-II upregulation in THP-1 cells, which can serve as surrogate dendritic cells (Supporting Information Figure S2). CD40L alone indeed induced increased expression, and this effect was concentration-dependently inhibited by the tested compounds (**6**, **10**, and **11**) (Supporting Information Figure S2).

Cyto- and genotoxicity—In parallel with the above experiments, cytotoxicities were also evaluated using a standard MTT assay; on one hand, to assess the safety of these compounds, and on the other, to ensure that the effects seen are not due to cell toxicity effects. Except for the amine substituted compound **8**, which had no significant CD40–CD40L inhibitory activity anyway, and the carboxylic acid substituted **11**, which was the only compound lacking an aromatic sulfonic acid substituent, the other compounds showed no signs of cytotoxicity for concentrations of up to 100 and 200 μM. Among the most active compounds that were also tested in cell-based assays (**6**, **10**, and **11**), only **11** showed a significant effect on viability at 100 μM (Supporting Information Figure S3). The mutagenic potential was also assessed for two compounds (**6** and **10**) using the Muta-Chromplate assay, which is a 96-well micro-plate version of the *Salmonella typhimurium* Ames test. As shown in Supporting Information Figure S4, neither of these compounds was found to have genotoxic potential as assessed by this assay for the concentrations tested of up to 500 μM.

Inhibition of CD40L-induced B cell proliferation—CD40 stimulation is an important signal for B cell proliferation, and soluble CD40L can induce proliferation of human B cells in a concentration-dependent manner. As before[67, 68], we used a CD40L-induced proliferation of primary human B cells assay to assess the inhibitory effect of our new small-molecule compounds. As Supporting Information Figure S5 shows, CD40L-induced B cell proliferation was concentration-dependently inhibited by compounds **6**, **10**, and **11** in statistically significant manner at concentrations higher than 10 μM. As expected, the CD40L antibody included as a positive control showed inhibitory activity with a half-maximal inhibitory concentration of about 1 nM in a manner consistent with our previous results[68].

Inhibition of CD40L-induced B cell activation—As an even more relevant activity assessment, we tested the ability of compounds **6**, **10**, and **11** to block CD40L-induced functional activation of primary B cells. Immunoglobulin class switch DNA recombination (CSR) and somatic hypermutation (SHM), which are critical for the maturation of antibody responses to antigens in B cells, are tightly controlled by the activity of activation-induced cytidine deaminase (AID)[85]. AID is encoded by the *AICDA* gene that is exclusively expressed in B cells and is necessary for opening the DNA molecule in the switch (S) regions in order to allow CSR. The expression of AID is tightly regulated by multiple repressive and enhancing elements. Engagement of CD40, which is constitutively expressed on the surface of B cells, with CD40L on T cells has been shown to positively regulate the expression of AID in B cells through activation of NF-κB signaling pathway ([85] and references therein). In particular, CD40-initiated NF-κB activation has been shown to synergize with interleukin-4 (IL-4) mediated STAT6 signaling to induce optimal AID expression[86]. To further validate the activity of our CD40–CD40L small-molecule inhibitors, we generated an aicda-lentiviral construct containing the promoter and enhancer region of aicda fused to the reporter Ds-Red, and used it to transfect human B cells isolated from healthy donors. In these cells, regulation of AID expression through CD40–CD40L signaling following incubation at different conditions can be evaluated by Ds-Red level assessed via flow cytometry. As shown in Figure 6, IL-4 alone failed to induce AID expression (<5% Ds-Red positive cells), but addition of CD40L produced good activation

(>25%). This was blocked by the CD40L antibody (mAb) used as a positive control (at a single concentration), and it was concentration-dependently blocked by compounds **6**, **10**, and **11** with IC_{50}s of 13.2, 4.5, and 15.9 μM, respectively (Figure 6, Table 1). A set of representative flow cytometry histograms illustrating the concentration-dependent response obtained for compound **10** are shown in Supporting Information Figure S6. These are particularly encouraging results as they were achieved using a true functional activity readout and they were obtained in primary human cells.

In Vivo Activity

Skin transplant model—A brief pharmacokinetic evaluation of compound **10** in mice indicated that, even if elimination is relatively fast (elimination half-life, $t_{1/2}$, in plasma of approximately 2 h), effective concentrations can be reached following systemic administration (Figure 7). Consequently, as a first *in vivo* test of the immunomodulating ability of the present compounds, we examined if compound **10** could cause prolongation of skin allograft survival using a model similar to that of Pinelli and co-workers[87]. Skin transplants are among the most stringent transplants as they are known to generate higher immune response than, liver, heart, or kidney transplants[88]. Skin grafts from Balb/c mice were transplanted in C57BL/6 mice that were treated with CTLA4-Ig plus either a CD40L antibody (MR-1) as a positive control or compound **10** (30 mg/kg) (daily, s.c.; in 20% hydroxypropyl-β-cyclodextrin, HPβCD). Mice treated with CTLA4-Ig alone rejected skin grafts with a mean survival time (MST) of 12.0 days. Addition of **10** prolonged survival in a statistically significant manner (MST of 15 days), but less than the positive control MR-1 (MST of 19 days) (Figure 8). There were no signs of toxicity during the two week chronic treatment with **10**.

Inhibition of alloantigen-induced immune response—The local administration of alloantigens induces T cell expansion in the draining lymph nodes (DLNs), and the ability of test compounds to inhibit this is an indication of their immunosuppressive potency. To test the activity of our compounds, we used a model[34] in which splenocytes isolated from DBA-2 mice were injected in the footpad of Balb/c recipients causing a significant (approximately eight-fold) increase in the number of cells in the draining popliteal lymph node by day 3. Compound **10** (20–60 mg/kg; s.c.; b.i.d.) significantly inhibited this in a dose-responsive manner and approaching the efficacy of the MR-1 anti-CD40L antibody used as a positive control (Figure 9).

DISCUSSION

Identification of small-molecules capable of costimulatory modulation as possible IM agents is of considerable interest. They could offer alternatives to antibodies and make oral administration possible. Several peptides interfering with the CD40–CD40L interaction with varying degrees of efficacy have been reported[19, 39, 89–91]; however, they are also unlikely to lead to therapeutics with adequate oral bioavailability. Finding small molecules that can interfere with costimulatory PPIs is undeniably challenging, but for TNFSF PPIs, several have been identified recently that provide at least proof-of-principle evidence that such modulation is possible, even if none have yet advanced to clinical development[62]. Here, we

report the first drug-like small molecules that have been shown to inhibit the CD40–CD40L interaction with low micromolar potency. In the cell-free binding inhibitory assay (Figure 4), several compounds showed less than micromolar potency, e.g., IC_{50} values of less than 0.5 μM for **6**, **10**, and **11** (Table 1), which were selected for further testing. For comparison, we have also tested a set of CD40-targeting inhibitory peptides ($KGYY_{15}$) that have been reported to be effective in preventing T1D in NODs[19]. In our human CD40–CD40L binding assay, mouse $KGYY_{15}$ (VLQWAKKGYYTMKSN), which was used in the NOD prevention study, showed no inhibitory activity. Human $KGYY_{15}$ (VLQWA**E**KGYYTM**SN**N) showed some inhibition, but only with an IC_{50} of 154 μM (Supporting Information Figure S7).

Previous small-molecule CD40–CD40L inhibitors include organic dyes such as **1**–**4** identified by us[68, 69] and (*S*)-2-(2'-(biphenyl-3-ylmethylcarbamoyl)-6,6'-bis((*S*)-2-(pyrrolidin-1-ylmethyl)pyrrolidine-1-carbonyl)-4,4'-bipyridine-2-carboxamido)-2-cyclohexylacetic acid (BIO8898), a large structure with a 4,4'-bipyridine core and four arms, identified by Silvian and co-workers at Biogen[92]. With compounds of the present study (**5**–**11**), there is evidence of adequate selectivity and specificity (Table 1), and several structural elements required for CD40–CD40L inhibitory activity have been identified. Among others, they include a chain of aromatic rings, which is often seen in PPI inhibitors in general. While a single-ring linker seemed to work in some of the azo dyes (e.g., **3** and **4**), a linker with two aromatic rings (i.e., chain of four aromatic rings) seems to be needed for our new amide-linked structures (e.g., **6** vs **5**). Presence of polar substituents at both ends is also needed for activity: compounds with an unsubstituted or chlorine-substituted naphthalene ring as well as compounds without a polar substituent on the terminal phenyl ring at the opposite end were inactive (data not shown). For the sulfonyl substituent, position 1 seems to be somewhat favored (e.g., **6** vs. **7**), and –COOH could be an adequate substitution (*cf.* **11**). At the other 4' end, several substituents can maintain activity, e.g., nitro (**6**), triazole (**9**), or ester (**10**) (Table 1), but amine (**8**) or halogen substituted compound completely lose CD40L inhibitory activity. All these agree well with the general observation that biphenyl scaffolds and acidic (e.g., –COOH) moieties seem to be present with high frequency among good protein binders[93]. It has also been suggested that chains of aromatic rings could act as α-helix mimetics and so are particularly well suited to interfere with PPIs[94, 95]. For our previous inhibitory compounds, including **1**–**4**, we have shown that they bind to CD40L and not to CD40[68], most likely in an allosteric manner interfering with the trimeric structure of these proteins (all TNFSF receptors and ligands bind as trimers; Figure 1). Considering their overall structural similarity (*cf.* Figure 3 and Figure 2) and their ability to inhibit the binding of CD40L to Mac-1 as well (Supporting Information Figure S1), it is reasonable to assume that the present compounds (**6**–**11**) also bind to CD40L.

All tested compounds concentration-dependently inhibited the CD40L-mediated activation of NF-κB sensor cells (Figure 5), of THP-1 cells, which can serve as surrogate dendritic cells (Supporting Information Figure S2), as well as the proliferation and activation of primary human B cells (Supporting Information Figure S5, Figure 6) and did so at concentration levels that are below cytotoxic levels (Supporting Information Figure S3, Table 1). While activity seems to be less than in the cell-free binding assay, most likely due to nonspecific binding to proteins, activities obtained are still better than those obtained for

the dye compounds before[68]. Hydrophobicity might also cause solubility limitations; measured water solubilities indicate that this could be a possible issue for compound **6** and **11** (with solubilities of 7 and 17 μM, respectively), but not **10**, which has a water solubility of 240 μM. Immunomodulatory activity has also been confirmed *in vivo* in a rodent skin transplant experiment (Figure 8) and in an alloantigen-induced T cell expansion model (draining popliteal lymph node; Figure 9). Prolongation of the skin graft was less than that obtained with the CD40 murine antibody, but promising enough for a once-a-day administration treatment regimen considering the relatively fast elimination of the tested compound (**10**). Notably, the same compound (**10**) was able to inhibit the alloantigen-induced T cell response in a draining lymph node in a dose responsive manner when administered b.i.d. for three days. These results are particularly encouraging for prospective IM treatments since CD40 stimulation is an important signal for many cells involved in immune responses including T cells, B cells, or dendritic cells, which act as APCs[96]. Results obtained here also confirm our original hypothesis[57, 68] that the chemical space of organic dyes can serve as a good starting point to identify PPI inhibitors in general. Such dyes are likely to show good protein binding affinity; many of them are used for tissue staining and can often achieve tissue specificity. Most azo dyes are likely to be within the chemical space of 'privileged structures' for protein binding (to the degree that such a space exists)[95, 97]. Because of their strong color, however, they are unsuitable for therapeutic development, and they are also susceptible to quick metabolic degradation by intestinal microorganisms and hepatic enzymes[98, 99]. The present results confirm that 'colorless' versions can be developed (e.g., by replacing the azo chromophores with amide linkers) while still maintaining good PPI inhibitory activity. It is also noteworthy that the present compounds achieve CD40–CD40L inhibitory activity with relatively small structures (molecular weights in the 500–600 dalton range). Typical PPI inhibitors tend to require larger structures to achieve sufficient activity with molecular weight that are in flagrant violation of the Lipinski rule-of-five (i.e., MW < 500)[100], which serves as a widely used guide to achieve oral bioavailability and an adequate pharmacokinetic profile.

The relatively small structures here (compared to other PPI inhibitors) also mean improved ligand binding efficiency. Ligand efficiency (LE) is defined as the binding energy per unit size, typically, the binding free energy per non-hydrogen atom: $LE = \Delta G^0/N_{nHa}$[101]. For small-molecule PPI inhibitors, LE tends to be in the 1.0 kJ/atom range[51, 57, 61] – less than the average LE of around 1.5 kJ/atom seen for usual protein-ligand interactions[101–104]. For reference purposes, an LE of 1.5 kJ/atom means an approximate doubling of affinity (halving of K_d or IC_{50}) with the addition of each non-hydrogen atom. For the present compounds (**6**, **10**, and **11**), LE is in the 0.91–0.93 kJ/atom range, similar to that of typical PPI inhibitors, and much better than LE of the larger and less potent **1** (0.4 kJ/atom).

CONCLUSIONS

In conclusion, by starting from the chemical space of organic dyes and using an iterative design, synthesize, test, and re-design approach, we have identified a set of new drug-like small-molecule inhibitors of the CD40–CD40L interaction (e.g., **6** or **10**). Their ability to inhibit CD40L-induced activation has been confirmed in cell-based assays including primary human B cells and in a rodent skin transplant experiment. Activities are in the low-

micromolar range, which might require further optimization; nevertheless, the present work provides clear proof-of-principle evidence that the CD40–CD40L costimulatory interaction, an important immunomodulatory and anti-inflammatory target, is susceptible to small-molecule inhibition.

EXPERIMENTAL SECTION

Materials

Chemicals and reagents used were obtained from Sigma-Aldrich (St. Louis, MO) except as indicated. Direct red 80 was from Santa Cruz Biotechnology (Dallas, TX). Recombinant receptors (hCD40:Fc, CD40:COMP, and TNF-R1:Fc) and tagged ligands (hCD154, hCD154:Fc, *Mega*CD40L, and TNF-α), were obtained from Enzo Life Sciences (San Diego, CA). Mac-1 (recombinant human integrin $\alpha_M\beta_2$ protein) and the monoclonal anti-human CD154 (clone 40804) and anti-human TNF-α antibodies (clone 1825) were obtained from R&D Systems (Minneapolis, MN). Inhibitory peptides $KGYY_{15}$[19] were purchased from New England Peptide (Gardner, MA, USA).

Chemistry. General Methods

Commercial grade reagents and solvents were purchased from VWR (Radnor, PA) and Sigma-Aldrich (St. Louis, MO) and directly used without further purification. 4'-Nitro[1,1'-biphenyl]-4-carboxylic acid was synthesized by two steps as described in the literature[105]. All reactions were carried out in oven- or flame-dried glassware under an atmosphere of dry argon unless otherwise noted. Except as otherwise indicated, all reactions were magnetically stirred and monitored by analytical thin-layer chromatography (TLC) using Merck (Kenilworth, NJ) pre-coated silica gel plates with F_{254} indicator. Visualization was accomplished by UV light (256 nm) with a combination of potassium permanganate and/or vanillin solution as an indicator. Flash column chromatography was performed according to the method of Still[106] using silica gel 60 (mesh 230–400; EMD Milipore, Billerica, MA).

All newly synthesized compounds were characterized with ^{1}H NMR, ^{13}C NMR, high-resolution mass spectrometry (HRMS), and infrared (IR) spectroscopy – detailed data are provided below. Chemical shifts are reported in ppm relative to TMS. DMSO-d_6 (2.50 ppm) was used as a solvent for ^{1}H NMR and ^{13}C NMR. ^{1}H NMR and ^{13}C NMR spectra were recorded on Bruker Avance 300 (300 MHz ^{1}H), 400 (400 MHz ^{1}H, 100 MHz ^{13}C), and 500 (500 MHz ^{1}H, 125 MHz ^{13}C). Chemical shift values (δ) are reported in ppm relative to Me_4Si (δ 0.0 ppm) unless otherwise noted. Proton spectra are reported as δ (multiplicity, coupling constant *J*, number of protons). Multiplicities are indicated by *s* (singlet), *d* (doublet), *t* (triplet), *q* (quartet), *p* (quintet), *h* (septet), *m* (multiplet), and *br* (broad). IR spectra were recorded with a FT-IR spectrophotometer Paragon 1000 (Perkin Elmer). Mass spectra were obtained at the Mass Spectrometry Laboratory, Department of Chemistry, University of Florida (Gainesville, FL). Low-resolution ES (electron spray) mass spectra were carried out with Finnigan LCQ DECA/Agilent 1100 LC/MS mass spectrometer (Thermo Fisher Scientific, Waltham, MA). High-resolution mass spectra were recorded on an Agilent 6220 ESI TOF (Santa Clara, CA) mass spectrometer. Analysis of sample purity was performed on an Agilent (Palo Alto, CA) 1100 series HPLC system with a

Thermoscientific Hypurity C8 (5 μm; 2.1 × 100 mm + guard column). HPLC conditions were as follows: solvent A = water with 2 mM ammonium acetate, solvent B = methanol with 2 mM ammonium acetate, and flow rate = 0.2 mL/min. Compounds were eluted with a gradient of A:B = 80:20 at 0 min to 0:100 at 50 min. Purity was determined via integration of UV spectra at 254 nm, and all tested compounds have a purity of ≥95%. All target compounds **5**–**11** were tested as triethylamine salts unless otherwise stated.

Water solubilities were determined by preparing saturated solutions in distilled water and measuring their concentrations by HPLC using calibration solutions prepared by dissolving known amounts of compounds in 20% (w/v) 2-hydroxypropyl-β-cyclodextrin (HPβCD) aqueous solution. Analyses for this and for plasma concentrations were performed on a Hitachi (Tokyo, Japan) L-2000 series HPLC system with a Sigma-Aldrich Discovery C18 column (5 μm; 4.6 × 150 mm + Supelco guard column) using a 60:40 mobile phase of water:acetonitrile (both with 2.0 mM ammonium acetate, flow rate 0.25 mL/min) by injection of 5 μL samples using a Hitachi L-2200 auto-sampler and with detection at 254 nm.

8-(4-(4-Nitrobenzamido)benzamido)naphthalene-1-sulfonic acid (5)—Preparation of compound **5** followed the general synthetic scheme of Scheme 1 via the synthesis of specific intermediaries **17** and **18** as summarized in Supporting Information Scheme S1. The general procedure for the coupling reaction as described below for **17** was followed with 4-nitrobenzoic acid **16** (0.25 g, 1.47 mmol) and 8-(4-aminobenzamido)naphthalene-1-sulfonic acid (**18**) (0.50 g, 1.13 mmol) to give the triethylamine salt of the title compound **5** as a yellow solid (0.47 g, 70%) (>99.9% pure by HPLC analysis (UV spectra at 254 nm)). ^{1}H NMR (500 MHz, DMSO-d_6): δ 12.54 (s, 1H), 10.80 (s, 1H), 8.81 (br, 1H), 8.39 (d, J = 8.8 Hz, 2H), 8.31 (dd, J = 1.3, 7.2 Hz, 1H), 8.26-8.16 (m, 5H), 8.00 (dd, J = 1.1, 8.2 Hz, 1H), 7.92 (d, J = 8.7 Hz, 2H), 7.80 (dd, J = 1.0, 8.1 Hz, 1H), 7.57 (t, J = 7.8 Hz, 1H), 7.47 (t, J = 7.6 Hz, 1H), 3.07 (q, J = 7.2 Hz, 6H), 1.15 (t, J = 7.3 Hz, 9H); ^{13}C NMR (125 MHz, DMSO-d_6): δ 164.8, 164.2, 149.2, 141.8, 141.2, 140.5, 135.7, 133.4, 131.8, 131.0, 129.3, 128.9, 127.4, 125.8, 125.3, 124.0, 123.9, 123.6, 122.9, 119.3, 45.8, 8.6; FTIR (neat) ν_{max} 3235, 2999, 2685, 1677, 1638, 1589, 1515, 1490, 1434, 1403, 1342, 1294, 1254, 1230, 1186, 1148, 1132, 1099, 1038, 1010, 917, 845, 835, 821, 759, 719, 706, 691, 678 cm^{-1}; HRMS (ESI) [M-H]$^{-}$ calcd. for $C_{24}H_{16}N_3O_7S^-$, 490.0714; found, 490.0715.

8-(4'-(4-Nitrobenzamido)biphenyl-4-ylcarboxamido)naphthalene-1-sulfonic acid (6)—Preparation of compound **6** followed the general synthetic scheme of Scheme 1 via the synthesis of intermediaries **14** and **15**. The general procedure for coupling as described below for **17** was followed with 4-nitrobenzoic acid (**16**) (0.50 g, 3.0 mmol) and 8-(4'-aminobiphenyl-4-ylcarboxamido)naphthalene-1-sulfonic acid (**15**) (1.20 g, 2.3 mmol) to give the triethylamine salt of the title compound **6** as a yellow solid (1.35 g, 87%) (99.9% pure by HPLC analysis (UV spectra at 254 nm)). ^{1}H NMR (500 MHz, DMSO-d_6): δ 12.64 (s, 1H), 10.75 (s, 1H), 8.85 (br, 1H), 8.39 (d, J = 8.1 Hz, 2H), 8.36 - 8.16 (m, 6H), 8.02 (d, J = 8.2 Hz, 1H), 7.95 (d, J = 8.2 Hz, 2H), 7.91 - 7.81 (m, 5H), 7.59 (t, J = 7.7 Hz, 1H), 7.49 (t, J = 7.5 Hz, 1H), 3.07 (q, J = 7.2 Hz, 6H), 1.15 (t, J = 7.1 Hz, 9H); ^{13}C NMR (125 MHz, DMSO-d_6): δ 165.1, 164.1, 149.2, 142.0, 141.8, 140.6, 138.8, 135.8, 134.9, 134.2, 133.3,

132.0, 129.4, 128.8, 127.5, 127.3, 126.0, 125.9, 125.4, 124.4, 124.1, 123.7, 123.0, 120.8, 45.7, 8.7; FTIR (neat) ν_{max} 3360, 3017, 2714, 1679, 1666, 1592, 1521, 1489, 1432, 1416, 1398, 1340, 1321, 1279, 1235, 1194, 1152, 1131, 1102, 1038, 1009, 929, 895, 864, 852, 824, 761, 708, 675, 661 cm^{-1}; HRMS (ESI) $[M-H]^-$ calcd. for $C_{30}H_{20}N_3O_7S^-$, 566.1027; found, 566.1054. Estimated water solubility: 4.7 μg/mL (7.0 μM).

4-(4'-(4-Nitrobenzamido)biphenyl-4-ylcarboxamido)naphthalene-1-sulfonic acid (7)—Preparation of compound **7** involved the synthesis of specific intermediaries **19** and **20** as summarized in Supporting Information Scheme S2. The general procedure for coupling as described below for **17** was followed with 4'-(4-nitrobenzamido)biphenyl-4-carboxylic acid (**20**) (0.26 g, 0.55 mmol) and 4-amino-1-naphthalenesulfonic acid (**21**) (112 mg, 0.5 mmol) to give the triethylamine salt of the title compound **7** as a yellow solid (0.27 g, 80%) (>99.9% pure by HPLC analysis (UV spectra at 254 nm)). ^{1}H NMR (500 MHz, DMSO-d_6): δ 10.72 (s, 1H), 10.49 (s, 1H), 8.93 (dd, J = 2.1, 6.9 Hz, 1H), 8.83 (br, 1H), 8.40 (d, J = 8.7 Hz, 2H), 8.23 (d, J = 8.7 Hz, 2H), 8.20 (d, J = 8.3 Hz, 2H), 8.04 - 7.98 (m, 2H), 7.96 (d, J = 8.6 Hz, 2H), 7.90 (d, J = 8.3 Hz, 2H), 7.85 (d, J = 8.6 Hz, 2H), 7.58 - 7.51 (m, 3H), 3.09 (q, J = 7.3 Hz, 6H), 1.17 (t, J = 7.3 Hz, 9H); ^{13}C NMR (125 MHz, DMSO-d_6): δ 165.8, 164.1, 149.3, 142.6, 142.4, 140.6, 138.9, 134.9, 134.7, 132.9, 129.8, 129.6, 129.4, 128.6, 128.0, 127.3, 126.3, 125.7, 125.6, 124.2, 123.7, 123.2, 122.5, 120.8, 45.7, 8.7; FTIR (neat) ν_{max} 3304, 2999, 2703, 1649, 1599, 1562, 1527, 1482, 1455, 1418, 1345, 1327, 1306, 1262, 1220, 1177, 1160, 1104, 1040, 1004, 897, 866, 833, 796, 769, 758, 704, 684 cm^{-1}; HRMS (ESI) $[M+H]^+$ calcd. for $C_{30}H_{22}N_3O_7S^+$, 568.1173; found, 568.1161.

8-(4'-(4-Aminobenzamido)biphenyl-4-ylcarboxamido)naphthalene-1-sulfonic acid (8)—The general procedure for hydrogenation as described below for **18** was followed with 8-(4'-(4-nitrobenzamido)biphenyl-4-ylcarboxamido)naphthalene-1-sulfonic acid (**6**) (1.35 g, 2.0 mmol) to give the triethylamine salt of the title compound as a white solid (0.95 g, 75%) (98.4% pure by HPLC analysis (UV spectra at 254 nm)). ^{1}H NMR (500 MHz, DMSO-d_6): δ 12.63 (s, 1H), 9.91 (s, 1H), 8.80 (br, 1H), 8.32 (dd, J = 1.2, 7.2 Hz, 1H), 8.26 (d, J = 8.4 Hz, 2H), 8.20 (dd, J = 0.9, 7.6 Hz, 1H), 8.01 (dd, J = 1.1, 8.1 Hz, 1H), 7.92 (d, J = 8.6 Hz, 2H), 7.81 (d, J = 8.3 Hz, 3H), 7.76 (d, J = 8.6 Hz, 4H), 7.58 (t, J = 7.8 Hz, 1H), 7.48 (t, J = 7.6 Hz, 1H), 6.64 (d, J = 8.6 Hz, 2H), 5.80 (br, 2H), 3.06 (q, J = 7.1 Hz, 6H), 1.14 (t, J = 7.3 Hz, 9H); ^{13}C NMR (125 MHz, DMSO-d_6): δ 165.3, 165.1, 152.1, 142.2, 141.8, 139.8, 135.8, 133.9, 133.6, 133.3, 131.8, 129.4, 128.7, 127.4, 126.9, 125.9, 125.7, 125.3, 124.2, 124.0, 123.0, 121.1, 120.3, 112.7, 45.8, 8.6; FTIR (neat) ν_{max} 3412, 3344, 3243, 2990, 2689, 1635, 1600, 1558, 1534, 1475, 1430, 1415, 1397, 1338, 1297, 1278, 1237, 1198, 1173, 1134, 1102, 1040, 1011, 928, 904, 845, 831, 820, 790, 762, 740, 720, 696, 670 cm^{-1}; HRMS (ESI) $[M-H]^-$ calcd. for $C_{30}H_{22}N_3O_5S^-$, 536.1286; found, 536.1299.

8-(4'-(1H-Benzo[d][1,2,3]triazole-5-carboxamido)biphenyl-4-ylcarboxamido)naphthalene-1-sulfonic acid (9)—The general procedure for coupling reaction as described below for **17** was followed with 1H-benzo[d][1,2,3]triazole-5-carboxylic acid (77 mg, 0.47 mmol) and 8-(4'-aminobiphenyl-4-ylcarboxamido)naphthalene-1-sulfonic acid (**15**) (0.21 g, 0.39 mmol) to give the triethylamine salt of the title compound as a white solid (180 mg, 69%) (99.0% pure by

HPLC analysis (UV spectra at 254 nm)). ^{1}H NMR (500 MHz, DMSO-d_6): δ 12.65 (s, 1H), 10.57 (s, 1H), 8.67 (s, 1H), 8.32 (dd, J = 0.8, 7.2 Hz, 1H), 8.27 (d, J = 8.4, 2H), 8.21 (d, J = 7.1 Hz, 1H), 8.08 (d, J = 9.3 Hz, 1H), 8.05 - 7.96 (m, 4H), 7.87 - 7.80 (m, 5H), 7.58 (t, J = 7.8 Hz, 1H), 7.48 (t, J = 7.7 Hz, 1H), 3.34 (br, 2H), 3.06 (q, J = 7.3 Hz, 6H), 1.15 (t, J = 7.3 Hz, 9H); ^{13}C NMR (125 MHz, DMSO-d_6): δ 165.2, 165.1, 142.0, 141.8, 139.2, 135.8, 134.5, 134.1, 133.3, 131.8, 128.8, 127.4, 127.1, 125.9, 125.8, 125.3, 124.2, 124.0, 123.0, 120.7, 45.8, 8.6; FTIR (neat) ν_{max} 3294, 3027, 1654, 1593, 1562, 1528, 1477, 1412, 1400, 1345, 1321, 1302, 1277, 1247, 1209, 1196, 1164, 1129, 1043, 1013, 935, 919, 881, 862, 837, 822, 799, 759, 742, 723, 662 cm^{-1}; HRMS (ESI) [M-H]$^-$ calcd. for $C_{30}H_{20}N_5O_5S^-$, 562.1191; found, 562.1197.

8-(4'-(4-(Methoxycarbonyl)benzamido)biphenyl-4-ylcarboxamido)naphthalene-1-sulfonic acid (10)—The general procedure for coupling as described below for **17** was followed with mono-methyl terephthalate (0.28 g, 15.7 mmol) and 8-(4'-aminobiphenyl-4-ylcarboxamido)naphthalene-1-sulfonic acid (**15**) (0.63 g, 1.21 mmol) to give the triethylamine salt of the title compound as a white solid (0.69 g, 84%) (97.7% pure by HPLC analysis (UV spectra at 254 nm)). ^{1}H NMR (500 MHz, DMSO-d_6): δ 12.64 (s, 1H), 10.58 (s, 1H), 8.80 (br, 1H), 8.31 (dd, J = 1.1, 7.2 Hz, 1H), 8.27 (d, J = 8.4 Hz, 2H), 8.21 (d, J = 6.7 Hz, 1H), 8.12 (s, 4H), 8.01 (dd, J = 1.0, 8.1 Hz, 1H), 7.95 (d, J = 8.6 Hz, 2H), 7.89-7.77 (m, 5H), 7.58 (t, J = 7.9 Hz, 1H), 7.48 (t, J = 7.6 Hz, 1H), 3.91 (s, 3H), 3.07 (q, J = 7.1 Hz, 6H), 1.15 (t, J = 7.3 Hz, 9H); ^{13}C NMR (125 MHz, DMSO-d_6): δ 165.7, 165.0, 164.8, 142.0, 141.8, 139.0, 138.9, 135.8, 134.7, 134.1, 133.3, 132.1, 131.8, 129.2, 128.7, 128.1, 127.4, 127.1, 125.9, 125.8, 125.3, 124.2, 124.0, 123.0, 120.7, 52.4, 45.8, 8.6; FTIR (neat) ν_{max} 3255, 3005, 2706, 1719, 1671, 1655, 1595, 1522, 1490, 1417, 1330, 1274, 1164, 1106, 1038, 1010, 920, 899, 869, 827, 789, 763, 724, 708, 661cm^{-1}; HRMS (ESI) [M-H]$^-$ calcd. for $C_{32}H_{23}N_2O_7S^-$, 579.1231; found, 579.1254. Estimated water solubility: 163.8 μg/mL (240 μM).

4-(4'-(4-Nitrobenzamido)biphenyl-4-ylcarboxamido)-1-naphthoic acid (11)—Preparation of compound **11** followed the general synthetic scheme of Scheme 1 via the synthesis of specific intermediaries **23**, **24**, and **25** as summarized in Supporting Information Scheme S3. The general procedure for hydrogenation as described below for **18** was followed with 4-(4'-nitrobiphenyl-4-ylcarboxamido)-1-naphthoic acid (**25**) (60 mg, 0.145 mmol) to give the free amine (58 mg) without further purification. The general procedure for the coupling reaction of 4-nitrobenzoic acid (**16**) (33 mg, 0.2 mmol) and the free amine gave the title compound **11** as a yellow solid (54 mg, 71%) (>99.9% pure by HPLC analysis (UV spectra at 254 nm)). ^{1}H NMR (400 MHz, DMSO-d_6): δ 13.11 (br, 1H), 10.71 (s, 1H), 10.63 (s, 1H), 8.98 (d, J = 8.5 Hz, 1H), 8.40 (d, J = 8.7 Hz, 2H), 8.27 - 8.15 (m, 6H), 7.96 (d, J = 8.6 Hz, 2H), 7.91 (d, J = 8.3 Hz, 2H). 7.85 (d, J = 8.7 Hz, 2H), 7.80 (d, J = 7.9 Hz, 1H), 7.70 (t, J = 7.5 Hz, 1H), 7.64 (t, J = 7.6 Hz, 1H); ^{13}C NMR (125 MHz, DMSO-d_6): δ 165.9, 164.0, 149.2, 142.7, 140.5, 138.9, 136.8, 134.6, 132.8, 131.7, 129.3, 129.1, 128.8, 128.7, 128.6, 127.2, 126.9, 126.5, 126.2, 125.7, 124.9, 123.60, 123.56, 122.4, 120.8; FTIR (neat) ν_{max} 3283, 1673, 1648, 1598, 1519, 1492, 1458, 1416, 1347, 1328, 1292, 1243, 1196, 1107, 913, 822, 764, 713, 684 cm^{-1}; HRMS (ESI) [M-H]$^-$ calcd. for $C_{31}H_{20}N_3O_6^-$, 530.1358; found, 530.1348. Estimated water solubility: 9.3 μg/mL (17.6 μM).

8-(4'-Nitrobiphenyl-4-ylcarboxamido)naphthalene-1-sulfonic acid (14)—The general procedure for the coupling reaction as described below for **17** was followed with 8-amino-1-naphthalenesulfonic acid (**12**) (1.50 g, 6.7 mmol) and 4'-nitro[1,1'-biphenyl]-4-carboxylic acid (**13**) (1.63 g, 6.7 mmol) to give the triethylamine salt of **14** as a yellow solid (2.4 g, 66%). ^{1}H NMR (500 MHz, DMSO-d_6): δ 12.70 (s, 1H), 8.79 (br, 1H), 8.38 - 8.29 (m, 5H), 8.20 (d, J = 7.6 Hz, 1H), 8.09 (d, J = 8.8 Hz, 2H), 8.02 (d, J = 8.1 Hz, 1H), 7.95 (d, J = 8.4 Hz, 2H), 7.83 (d, J = 7.8 Hz, 1H), 7.59 (t, J = 7.9 Hz, 1H), 7.48 (t, J = 7.6 Hz, 1H), 3.08 (q, J = 7.2 Hz, 6H), 1.15 (t, J = 7.3 Hz, 9H); ^{13}C NMR (125 MHz, DMSO-d_6): δ 164.8, 147.0, 145.8, 141.8, 140.1, 135.9, 135.8, 133.2, 131.9, 128.9, 128.1, 127.4, 127.0, 126.1, 125.3, 124.2, 124.1, 124.0, 123.0, 45.8, 8.6; FTIR (neat) ν_{max} 3028, 2735, 1668, 1596, 1515, 1494, 1480, 1429, 1393, 1339, 1328, 1280, 1231, 1186, 1162, 1126, 1110, 1039, 1010, 924, 894, 869, 854, 843, 826, 788, 763, 740, 692 cm^{-1}; HRMS (ESI) $[M+H]^+$ calcd. for $C_{23}H_{17}N_2O_6S^+$, 449.0802; found, 449.0781.

8-(4'-Aminobiphenyl-4-ylcarboxamido)naphthalene-1-sulfonic acid (15)—The general procedure for hydrogenation as described below for **18** was followed with 8-(4'-nitrobiphenyl-4-ylcarboxamido)naphthalene-1-sulfonic acid (**14**) (2.8 g, 5.1 mmol) to give the triethylamine salt of **15** as a white solid (2.3 g, 86%). ^{1}H NMR (500 MHz, DMSO-d_6): δ 12.56 (s, 1H), 8.80 (br, 1H), 8.31 (dd, J = 1.1, 6.1 Hz, 1H), 8.25 - 8.12 (m, 3H), 8.00 (d, J = 7.2 Hz, 1H), 7.80 (d, J = 7.3 Hz, 1H), 7.67 (d, J = 8.3 Hz, 2H), 7.57 (t, J = 7.8 Hz, 1H), 7.49 (d, J = 7.0 Hz, 2H), 7.47 (t, J = 7.7 Hz, 1H), 6.68 (d, J = 8.4 Hz, 2H), 5.33 (s, 2H), 3.05 (q, J = 7.2 Hz, 6H), 1.14 (t, J = 7.3 Hz, 9H); ^{13}C NMR (125 MHz, DMSO-d_6): δ 165.2, 148.9, 143.1, 141.8, 135.7, 133.4, 132.5, 131.8, 128.6, 127.4, 127.3, 126.3, 125.7, 125.3, 124.6, 124.1, 123.9, 123.0, 114.2, 45.7, 8.6; FTIR (neat) ν_{max} 3431, 3338, 3227, 3006, 2712, 1648, 1602, 1531, 1492, 1474, 1429, 1397, 1331, 1284, 1227, 1196, 1184, 1161, 1061, 1036, 1008, 921, 891, 823, 788, 761, 725, 704, 663 cm^{-1}; HRMS (ESI) $[M+H]^+$ calcd. for $C_{23}H_{19}N_2O_4S^+$, 419.1060; found, 419.1058.

8-(4-nitrobenzamido)naphthalene-1-sulfonic acid (17) and general procedure for the coupling reaction—For the synthesis of **17** and as a general procedure of coupling a modified version of the coupling reaction from reference[74] was used. Under an argon atmosphere, trimethylamine (1.74 mL, 12.5 mmol) was added dropwise to a mixture of 4-nitrobenzoic acid **16** (1.09 g, 6.5 mmol), *O*-(6-chlorobenzotriazol-1-yl)-*N, N, N', N'*-tetramethyluronium hexafluorophosphate HCTU (2.7 g, 6.5 mmol) and DMF (10 mL) at 0°C and the resulting reaction mixture was stirred for 1 h at the same temperature. Subsequently, 8-amino-1-naphthalenesulfonic acid **12** (1.12 g, 5.0 mmol) was added at the same temperature. The resulting reaction mixture was allowed to stir overnight at room temperature (RT). Diethyl ether (50 mL) was added to the reaction mixture, and a yellow precipitate formed. This precipitate was collected by filtration and washed with diethyl ether (3 × 10 mL) to afford the triethylamine salt of **17** as a yellow solid (2.0 g, 65%). ^{1}H NMR (500 MHz, DMSO-d_6): δ 12.83 (s, 1H), 8.82 (br, 1H), 8.39 (d, J = 9.0 Hz, 2H), 8.36 (d, J = 8.9 Hz, 2H), 8.30 (dd, J = 1.2, 7.2 Hz, 1H), 8.17 (d, J = 7.6 Hz, 1H), 8.03 (dd, J = 0.9, 8.1 Hz, 1H), 7.86 (d, J = 8.1 Hz, 1H), 7.60 (t, J = 7.8, 1H), 7.49 (t, J = 7.4 Hz, 1H), 3.08 (q, J = 7.2 Hz, 6H), 1.15 (t, J = 7.3 Hz, 9H); ^{13}C NMR (125 MHz, DMSO-d_6): δ 163.9, 148.9, 141.6, 141.5, 135.7, 132.7, 131.9, 129.4, 127.5, 126.5, 125.3, 124.3, 124.1, 123.3, 122.9,

45.8, 8.6; FTIR (neat) ν_{max} 3244, 3013, 2714, 1675, 1602, 1519, 1489, 1454, 1432, 1391, 1347, 1337, 1277, 1241, 1198, 1164, 1128, 1039, 1010, 916, 880, 853, 824, 782, 763, 713 cm^{-1}; HRMS $[M+H]^+$ calcd. for $C_{17}H_{13}N_2O_6S^+$, 373.0489; found, 373.0479.

8-(4-aminobenzamido)naphthalene-1-sulfonic acid (18) and general procedure for the hydrogenation reaction—For the synthesis of **18** and as a general procedure of coupling a modified version of the hydrogenation reaction from reference[75] was used. A mixture of 8-(4-nitrobenzamido)naphthalene-1-sulfonic acid (**17**) (0.82 g, 1.73 mmol) and 10% Pd on carbon (27 mg) in a solvent mixture of EtOH (2.0 mL) and DMF (1.0 mL) was hydrogenated (H_2 balloon) at 80°C for 3.5 h. The reaction mixture was filtered via a short pad of Celite®, concentrated *in vacuo*, and recrystallized from MeOH to afford the triethylamine salt of **18** as a white solid (0.61 g, 80%). ^{1}H NMR (500 MHz, DMSO-d_6): δ 12.22 (s, 1H), 8.86 (br, 1H), 8.28 (d, J = 6.1 Hz, 1H), 8.14 (d, J = 6.7 Hz, 1H), 7.96 (d, J = 7.4 Hz, 1H), 7.92 (d, J = 8.6 Hz, 2H), 7.73 (d, J = 7.3 Hz, 1H), 7.51 (t, J = 7.8 Hz, 1H), 7.43 (t, J = 7.7 Hz, 1H), 6.64 (d, J = 8.5 Hz, 2H), 3.38 (br, 2H), 3.06 (q, J = 7.1 Hz, 6H), 1.15 (t, J = 7.2 Hz, 9H); ^{13}C NMR (125 MHz, DMSO-d_6): δ 165.3, 150.5, 141.9, 135.8, 133.9, 131.8, 129.8, 127.2, 125.3, 125.2, 123.9, 123.8, 123.2, 122.9, 113.1, 45.8, 8.6; FTIR (neat) ν_{max} 3343, 3228, 1656, 1627, 1602, 1571, 1539, 1515, 1495, 1430, 1389, 1336, 1278, 1174, 1132, 1106, 1091, 1044, 1016, 918, 843, 820, 784, 754, 676cm^{-1}; HRMS $[M+Na]^+$ calcd. for $C_{17}H_{14}N_2NaO_4S^+$, 365.0566; found, 365.0555.

4'-Aminobiphenyl-4-carboxylic acid (19)—The general procedure for hydrogenation as described earlier for **18** was followed with 4'-nitrobiphenyl-4-carboxylic acid (**13**) (243 mg, 1.0 mmol) to give **19** as a white solid (109 mg, 51%). ^{1}H NMR (500 MHz, DMSO-d_6): δ 12.6 (br, 1H), 7.93 (d, J = 8.5 Hz, 2H), 7.67 (d, J = 8.4 Hz, 2H), 7.46 (d, J = 8.6 Hz, 2H), 6.67 (d, J = 8.6 Hz, 2H), 5.42 (br, 2H); ^{13}C NMR (125 MHz, DMSO-d_6): δ 167.3, 149.3, 144.8, 129.9, 127.6, 127.6, 125.8, 125.0, 114.2; FTIR (neat) ν_{max} 3327, 3179, 2636, 1679, 1598, 1530, 1492, 1398, 1337, 1262, 1231, 1145, 1022, 949, 928, 863, 830, 774, 726, 701 cm^{-1}; HRMS (ESI) $[M+H]^+$ calcd. for $C_{13}H_{12}NO_2^+$, 214.0863; found, 214.0872.

4'-(4-Nitrobenzamido)biphenyl-4-carboxylic acid (20)—The general procedure for coupling reaction as described earlier for **17** was followed with 4-nitrobenzoic acid (**16**) (2.8 g, 16.6 mmol) and 4'-aminobiphenyl-4-carboxylic acid (**19**) (2.4 g, 11.3 mmol) to give **20** as a yellow solid (3.8 g, 73%). ^{1}H NMR (500 MHz, DMSO-d_6): δ 12.94 (br, 1H), 10.70 (s, 1H), 8.39 (d, J = 8.6 Hz, 2H), 8.22 (d, J = 8.7 Hz, 2H), 8.02 (d, J = 8.2 Hz, 2H), 7.93 (d, J = 8.5 Hz, 2H), 7.82 (d, J = 8.2 Hz, 2H), 7.80 (d, J = 8.5 Hz, 2H); ^{13}C NMR (125 MHz, DMSO-d_6): δ 167.1, 164.0, 149.2, 143.7, 140.5, 139.0, 134.5, 130.0, 129.27, 129.26, 127.3, 126.3, 123.6, 120.8; FTIR (neat) ν_{max} 3301, 1694, 1632, 1593, 1569, 1515, 1419, 1391, 1347, 1330, 1301, 1255, 1199, 1107, 1005, 870, 856, 826, 798, 773, 712, 701, 672 cm^{-1}; HRMS (ESI) $[M+H]^+$ calcd. for $C_{20}H_{15}N_2O_5^+$, 363.0975; found, 363.0971.

Methyl 4-amino-1-naphthoate (23)—For the synthesis of **23**, a modified version of the esterification reaction from reference[107] was used. Thionyl chloride (7.8 mL, 107 mmol) was added dropwise to a suspension of 4-amino-1-naphthoic acid (1.0 g, 5.3 mmol) and MeOH (10 mL) at 0°C. The reaction mixture was stirred overnight at 50°C and then

concentrated *in vacuo*. This crude material was purified by flash chromatography on silica gel (25% dichloromethane in hexane) to afford **23** as a brown solid (0.29 g, 27%). ^{1}H NMR (500 MHz, DMSO-d_6): δ 9.15 (d, J = 8.5 Hz, 1H), 8.15 (d, J = 8.0 Hz, 1H), 7.80 (d, J = 8.2 Hz, 1H), 7.60 (t, J = 7.1 Hz, 1H), 7.48 (t, J = 7.2 Hz, 1H), 6.71 (d, J = 8.0 Hz, 1H), 4.58 (s, 2H), 3.93 (s, 3H). ^{13}C NMR (125 MHz, DMSO-d_6): δ 168.0, 147.4, 133.4, 132.9, 128.1, 126.9, 125.1, 122.8, 120.8, 116.3, 107.6, 51.7; FTIR (neat) ν_{max} 3491, 3363, 3241, 1682, 1631, 1568, 1517, 1473, 1435, 1349, 1267, 1236, 1198, 1165, 1132, 1034, 1014, 925, 839, 788, 764 cm^{-1}; HRMS [M+Na]$^{+}$ calcd. for $C_{12}H_{11}NNaO_2^{+}$, 224.0682; found, 224.0690.

Methyl 4-(4'-nitrobiphenyl-4-ylcarboxamido)-1-naphthoate (24)—The general procedure for coupling as described earlier for **17** was followed with 4'-nitro[1,1'-biphenyl]-4-carboxylic acid (**13**) (0.28 g, 1.14 mmol) and methyl 4-amino-1-naphthoate (**23**) (0.22 g, 0.108 mmol) to give **24** as a yellow solid (130 mg, 28%). ^{1}H NMR (500 MHz, DMSO-d_6): δ 10.74 (s, 1H), 8.86 (d, J = 8.6 Hz, 1H), 8.36 (d, J = 8.8 Hz, 2H), 8.26 (d, J = 8.4 Hz, 2H), 8.24 – 8.18 (m, 2H), 8.09 (d, J = 8.8 Hz, 2H), 8.01 (d, J = 8.4 Hz, 2H), 7.84 (d, J = 7.9 Hz, 1H), 7.72 (dt, J = 0.9, 7.1 Hz, 1H), 7.66 (dt, J = 0.8, 7.0 Hz, 1H), 3.97 (s, 3H). ^{13}C NMR (125 MHz, DMSO-d_6): δ 167.0, 165.7, 147.1, 145.5, 140.9, 138.4, 134.4, 131.4, 129.9, 128.8, 128.2, 127.9, 127.4, 126.3, 125.4, 124.4, 124.2, 123.9, 122.0, 52.2. ; FTIR (neat) ν_{max} 3436, 1698, 1676, 1596, 1524, 1494, 1484, 1458, 1435, 1393, 1330, 1286, 1240, 1196, 1177, 1139, 1109, 1039, 1004, 903, 869, 855, 845, 830, 813, 794, 778, 739, 690, 677 cm^{-1}; HRMS [M+Na]$^{+}$ calcd. for $C_{25}H_{18}N_2NaO_5^{+}$, 449.1108; found, 449.1089.

4-(4'-Nitrobiphenyl-4-ylcarboxamido)-1-naphthoic acid (25)—For the synthesis of **25**, a modified version of the hydration reaction from reference[105] was used. A solution of sodium hydroxide (60 mg, 1.50 mmol) in water (0.2 mL) was added dropwise to a solution of methyl 4-(4'-nitrobiphenyl-4-ylcarboxamido)-1-naphthoate (**24**) (130 mg, 0.30 mmol) in tetrahydrofuran (2.0 mL) and methanol (0.2 mL). The resulting mixture was warmed up and stirred overnight at 50°C. The solvents were removed under vacuum. Water (2.0 mL) was added, and the pH of the resulting mixture was adjusted to 2.0. The precipitate was collected by filtration and washed with Et_2O (3 × 2.0 mL) to afford **25** as a yellow solid (76 mg, 59%). ^{1}H NMR (500 MHz, DMSO-d_6): δ 13.14 (br, 1H), 10.73 (s, 1H), 8.98 (d, J = 8.6 Hz, 1H), 8.36 (d, J = 8.6 Hz, 2H), 8.27 (d, J = 8.2 Hz, 2H), 8.23 (d, J = 7.8 Hz, 1H), 8.18 (d, J = 8.4 Hz, 1H), 8.09 (d, J = 8.6 Hz, 2H), 8.01 (d, J = 8.1 Hz, 2H), 7.80 (d, J = 7.9 Hz, 1H), 7.70 (t, J = 7.2 Hz, 1H), 7.64 (t, J =7.8 Hz, 1H). ^{13}C NMR (125 MHz, DMSO-d_6): δ 168.4, 165.7, 147.1, 145.5, 140.9, 138.0, 134.4, 131.7, 129.8, 128.9, 128.8, 128.3, 127.5, 127.4, 125.8, 125.6, 124.2, 123.8, 122.3, 122.1. ; FTIR (neat) ν_{max} 2936, 2614, 1674, 1596, 1577, 1498, 1482, 1457, 1426, 1396, 1383, 1334, 1286, 1235, 1201, 1140, 1109, 1005, 982, 912, 856, 837, 793, 781, 769, 739, 689, 677 cm^{-1}; HRMS [M+Na]$^{+}$ calcd. for $C_{24}H_{16}N_2NaO_5^{+}$, 435.0951; found, 435.0931.

Binding Assays

Binding inhibition assays were performed in a 96-well cell-free format as described before[68, 70]. Briefly, microtiter plates (Nunc F Maxisorp, 96-well; Thermo Fisher Scientific, Waltham, MA) were coated overnight at 4°C with 100 μL/well of Fc-conjugated receptors diluted in PBS 7.2. This was followed by blocking with 200 μL/well of blocking solution

(PBS 7.2, 0.05%Tween-20, 1% BSA) for 1 h at RT. Then, plates were washed twice using washing solution (PBS 7.4, 0.05% Tween-20) and tapped dry before the addition of the appropriate FLAG tagged / biotinylated ligands along with different concentrations of tested dyes diluted in binding buffer (100 mM HEPES, 0.005% BSA pH 7.2) to give a total volume of 100 μL/well. After 1 h incubation, three washes were conducted, and anti-FLAG HRP conjugate was used to detect the bound FLAG-tagged ligand. Plates were washed three times before the addition of 120 μL/well of HRP substrate TMB (3,3',5,5'-tetramethylbenzidine) and kept in the dark for 15–30 min. The reaction was stopped using 30 μL of 1M H_2SO_4, and the absorbance value was read at 450 nm. The concentrations of receptors used were 0.3 μg/mL for CD40 and TNF-R and 0.4 μg/mL for Mac-1. The concentrations of the ligands were fixed at 0.02 μg/mL for CD40L and TNF-α and 0.2 μg/mL for CD40L in the Mac-1 binding assay. These values were selected following preliminary testing to optimize response (i.e., to produce a high-enough signal at conditions close to half-maximal response, EC_{50}). Stock solutions of compounds at 10 mM in DMSO were used; DMSO concentrations below 3% were found to not cause any effect on the readouts. As before[68, 71], to verify that inhibition is not due to colloidal aggregation, CD40 binding inhibition was also measured in the presence of the non-ionic detergent Triton-X 100 (0.01%), as recommended for the detection of such effects[80, 81].

Cytotoxicity Assay

For the MTT assay, THP-1 human myeloid cells obtained from American Type Culture Collection (ATCC; Manasses, VA) were cultured in RPMI-1640 medium (Invitrogen, CA) with 10% FBS (v/v; Invitrogen) and 1% penicillin-streptomycin (v/v; Invitrogen). Cells were centrifuged and re-suspended in the same medium without FBS for a 24-hour starvation. Then cells were added to a 96-well microtiter plate at a density of 50,000 cells/well in the absence or presence of various concentrations of compounds diluted in the same media. The plate was incubated at 37°C for 48 hours. 20 μL per well of MTT (Promega, Madison, WI) was added to the culture after treatments, and cells were incubated at 37°C for another half an hour. Formazan levels were measured using a plate reader at 490 nm.

Mutagenicity Assay

Assessment of mutagenicity (Ames test) was performed using the Muta-Chromplate assay (Environmental Bio-Detection Products, Mississauga, Ontario, Canada) following the instructions of the manufacturer. Briefly, lyophilized *S. typhimurium* TA-100 was reconstituted in the provided growth media and incubated overnight (16–18 h) at 37°C, then 5 μL was dispensed to 20 mL of reaction mixture prepared with varying concentrations of test compounds (0.1 to 500 μM obtained using stock solution diluted in DMSO; the concentration of DMSO used did not exceed 2.5% of the final volume for any of the test conditions used). The reaction mixture was plated on 96-well microplates (one plate per condition), sealed in airtight sterile bags, incubated at 37°C and observed daily to count the number of positive wells. One plate each was used for background, positive control (NaN_3), and sterility check conditions, and significance levels were determined using the tables provided by the manufacturer.

Sensor Cell Assay

CD40 expressing NF-κB sensor cells (HEK Blue, InvivoGen, San Diego, CA) were used to assess the ability of the present compounds to block CD40L-induced activation as described before[70, 108]. Briefly, cells were maintained in DMEM at 80% confluence for each experiment. Cells were trypsinized and re-suspended in the same medium with 1% FBS and seeded on 96-well microtiter plates at a density of 1×10^5 cells/well in the absence and presence of various concentrations of compounds diluted in the same media. For ligand mediated stimulation, final concentrations of recombinant human CD40L (20 ng/mL), which has been selected following preliminary testing to optimize response, were maintained in the wells for this purpose. After 18-hour incubation at 37°C, 20 μL supernatant of each well were taken and added to another 96-well microtiter plate containing 180 μL/well of QUANTI-Blue (InvivoGen). The level of SEAP was determined after 30-minute incubation at 37°C by reading at 625 nm using a spectrophotometer. A monoclonal anti-human CD154 antibody (clone 40804, R&D Systems, Minneapolis, MN) was used as a positive control.

THP-1 Cell Assays

THP-1 human myeloid cells obtained from ATCC were cultivated in Roswell Park Memorial Institute (RPMI) media 1640 supplemented with 10% FBS, 100 U/mL penicillin, and streptomycin 100 μg/mL to a density of 1×10^6 cells per mL. Cells were centrifuged and cultured in the same medium without FBS for a period of 24 h. Starved cells were re-suspended in fresh medium without FBS and stimulated with 0.5 μg/mL of rhCD154 (MegaCD40L; Enzo Life Sciences) in the presence of various concentrations of test compounds. All cultivations were carried out at 37°C, 90% humidity, and 5% CO_2. After 48 h incubation, cells were stained with monoclonal antihuman HLA-DR antibody APC-Alexa Fluor® 750 (clone LN3; eBioscience, San Diego, CA) and subsequently with 6-diamidino-2-phenylindole (DAPI) immediately before flow cytometry analysis. Stained THP-1 and B cells were analyzed using a BD LSR II Flow Cytometer (BD Biosciences, San Jose, CA, USA). Cell surface markers were quantified in live cells only after gating out DAPI-labeled cells.

B Cell Isolation

PBMC from healthy donors were collected by density gradient centrifugation on LSM Lymphocyte Separation Medium (MP Biomedicals, Santa Ana, CA). Cells were then washed three times with medium (RPMI 1640). B cells were isolated from the PBMC as follows. Briefly, cells were washed three times with medium (RPMI 1640) and incubated for 20 min at 4°C with 20 μL/10^7 cells of anti-CD19 Microbeads (Miltenyi Biotech, Bergisch Gladbach, Germany), according to the MiniMacs protocol (Miltenyi Biotech). Cells were then purified using magnetic columns. Comparable numbers of $CD19^+$ cells were obtained after negative selection. At the end of the purification procedure, cells were found to be almost exclusively (>90%) $CD19^+$ by cytofluorimetric analysis.

B Cell Proliferation Assay

Inhibition of cell proliferation was determined using the colorimetric cell proliferation ELISA BrdU kit from Roche Applied Science (Indianapolis, IN) as described before[68].

Briefly, cells were cultured in 96 wells plates (100 μL/well) at a cell density of 2×10^5 cells/mL in IMDM medium supplemented with 10% FBS, 100 U/mL penicillin, streptomycin 100 μg/mL, insulin-transferrin-selenium-G (all materials from Invitrogen, San Diego, CA) and 0.2 μg/mL of rhIL-4 (Peprotech, Rocky Hill, NJ). Cells were activated with 0.1 μg/mL of rhCD154 (*Mega*CD40L, Enzo Life Sciences) in the presence of various concentrations of test compounds. After 48 h, BrdU labeling solution was added as recommended, and cells were cultivated for another 48 h. Detection of incorporated BrdU was carried out following the instructions of the ELISA BrdU kit.

B Cell Activation Assay

Preparation of the aicda-lentiviral constructs—The Lenti-X lentiviral vector system from Clontech was utilized for the AID promoter construction. The DsRed Lenti-X vector (Clontech, Mountain View, CA) was used as the positive control as it contains a CMV promoter. For the aicda-DsRed lentiviral vector, the CMV promoter was excised from the DsRed Lenti-X vector using ClaI and BamHI double digestion to obtain a linear plasmid. The Sp1 minimal promoter was designed with a ClaI site at the 5' end and a HindIII site at the 3' end (nnnnClaI-GGGGCGGGGC-HindIIInnn) synthesized by Sigma oligo synthesis services. The enhancer oligo was also designed to contain the Pax-5 and two E-box binding sites (nnnnHindIII-GGTCACGCCTCAGTGCCCaCAGCTGtctcagCAGCTG-BamHInnnn) and also synthesized by Sigma oligo synthesis services in order to create the inserts for the aicda-DsRed vector. The promoter and enhancer oligos were then ligated to the plasmid which was still linear at this point. After the promoter was ligated at the ClaI site and the enhancer was ligated at the BamHI site, a HindIII digestion was performed followed by DNA ligation to join the promoter and enhancer and close the plasmid. Ligation of the two fragments was carried out with a molar insert:vector ratio of 3:1 at 16°C overnight using the Quick Ligation Kit (NEB; Ipswich, MA). Transformation of supercompetent *E. coli* (Agilent Technologies-Stratagene; La Jolla, CA) was performed according to the protocol of the manufacturer. Transformed bacteria were grown on LB-Plates with ampicillin (100 μg/mL) and colonies were obtained for plasmid-preparation. Plasmid-DNA was tested by restriction digestion and PCR.

Transient transfection of the Lenti-X 293T packaging cells and viral production—The aicda-DsRed Lenti X vector was co-transfected with the packing mix vectors provided by Clontech into the LentiX 293T cells with the Xfect reagent according to the Clontech protocol. The viral supernatants were harvested 48 hours post transduction. The Lentivirus was concentrated using the LentiX concentrator from Clontech.

Lentiviral transduction—Concentrated lentivirus was used immediately or frozen at −80°C (for use within a week) for retroviral transduction of B cells. Lentiviral infections of B-cells were performed using the centrifugation method[109]. In brief, 7 to 14×10^6 peripheral blood B cells were re-suspended in 5 to 10 ml of lenti-viral supernatant with 8 μg/mL final concentration of polybreme (Sigma-Aldrich). The mixture was centrifuged in 6 well plates for 1.5 h at 2,500g at 32°C[109] in order to achieve close contact between the retroviral particles and the cells. After 24 h, the media was replaced with fresh RPMI complete (at 1×10^6 cells/mL), and cells were cultured at 37°C and 5% CO_2.

B cell activation assessment—1.25×10^5 cells/mL of transfected B cells were stimulated with IL-4 at 0.2 μg/mL and CD40 ligand at 0.2 μg/mL in IMDM media with 10% FBS. In addition, various concentrations of candidate compounds diluted in the same media were added along with the described condition above. Also, 1 μg/ml of CpG was used as positive control for activation. After culture for 2 days at 37°C and 5% CO_2, B cells were collected, and AID activation level as represented by the level of Ds-Red expression was assessed by flow cytometry using BD LSRFortessa cell analyzer.

Animal Care and Treatment

All mice used for these studies (C57BL/6, BALB/c, and DBA-2) were obtained from Jackson Laboratories (Bar Harbor, ME). All animal studies were reviewed and approved by the University of Miami Institutional Animal Care and Use Committee (Protocol no. 15-078). All procedures were conducted according to the guidelines of the Committee on Care and Use of Laboratory Animals, Institute of Laboratory Animal Resources (National Research Council, Washington DC). Animals were housed in microisolated cages in Virus Antibody Free rooms with free access to autoclaved food and water at the Department of Veterinary Resources of the University of Miami.

Pharmacokinetic Evaluation in Mice

Pharmacokinetic (PK) in mice was evaluated for compound **10** by quantifying plasma concentration from blood samples (50 μL) drawn from the tail at predefined time points (0, 0.5, 1, 2, 4, 6, and 24 h) following administration of a single dose (1.6 mg/mouse, ~60 mg/kg; s.c. in 250 μL of 20% w/v hydroxypropyl-β-cyclodextrin HPβCD solution) to C57BL/6 mice ($n = 4$; 10 week old males). Plasma concentrations were obtained using the HPLC method already described. In brief, a Hitachi L-2000 series HPLC system with a Sigma-Aldrich Discovery C18 column (5 μm; 4.6 × 150 mm + Supelco guard column) was used with a 60:40 mobile phase of water:acetonitrile at a flow rate of 0.25 mL/min, and 5 μL plasma samples were injected directly using a Hitachi L-2200 auto-sampler. Concentration were calculated from the corresponding peak areas (detection at 254 nm) following a calibration curve that indicated linear range in the 1 to 500 μg/mL range. Experimental concentration data obtained this way were fitted with a standard noncompartmental analyses as well as with a one compartment, first order absorption, first order elimination PK model using Phoenix™ WinNonlin® 6.0 (Pharsight Corp., St. Louis, MO) to estimate the elimination rate constant k_{10} and the corresponding elimination half-life, $t_{1/2} = \ln(2)/k_{10}$.

Skin Transplant

Full-thickness ear skins from donor mice (BALB/c) were transplanted onto the dorsal thorax of recipient mice (C57BL/6) by placing them on ~1 cm diameter graft beds and securing with bandages. Following a protocol from[87], mice were treated with CTLA4-Ig (Orencia; Bristol-Myers Squibb, New York City, NY; 250 μg, days 0, 2, 4, and 6 plus either CD40L antibody (MR-1; Bio X Cell; West Lebanon, NH; 250 μg, days 0, 2, 4, and 6) or **10** (30 mg/kg) (daily, s.c.). Due to solubility limitations, compound **10** was administered in 20% w/v hydroxypropyl-β-cyclodextrin (HPβCD) solution. Bandages were removed on day 7 post-transplant and grafts were monitored and scored daily. Skin grafts were rated visually

(0: perfect skin, 1: 10%– 50% necrotic, 2: 75% necrotic, 3: 100% necrotic), and the first score of 3 was considered as the day of rejection.

Draining Lymph Node

Ability to inhibit alloantigen-induced T cell response in a draining lymph node was tested following the protocol from[34]. In brief, BALB/c mice (10–12 week old, female) received a footpad injection of 1×10^7 splenocytes isolated from DBA-2 mice (10–12 week old, male). CD40L antibody (MR-1; 20 mg/kg, day -1 and 0) or compound **6** and **10** (20–60 mg/kg; b.i.d. from day −1 to 3, in 20% HPβCD) were administered s.c., and the draining popliteal nodes (DLNs) were collected 3 days after the alloantigen challenge. DLN cells were counted and data are shown as mean ± SD (n = 3–4 per group).

Statistics, Data Fitting

All binding inhibition and cell assays were tested in duplicate or triplicate per plates, and all assays were performed as at least three independent experiments. As before[70, 71], binding and cytotoxicity data were converted to percent inhibition and fitted with standard log inhibitor vs. normalized response models using nonlinear regression in GraphPad Prism (GraphPad, La Jolla, CA) to establish half-maximal (median) inhibitory IC_{50} or median lethal concentration (LC_{50}) values, $B = 100 \cdot [C]/([C]+IC_{50})$. Data from the sensor cell and B cell functional assays were fitted with a similar model that also allowed for a variable slope using the log inhibitor vs. normalized response (variable slope) model from Prism with a Hill slope (n) shared across all compounds, $B = 100 \cdot [C]^n/([C]^n + IC_{50}{}^n)$. Cell assays and draining lymph node data were analyzed by one-way repeated-measures analysis of variance (ANOVA) followed by Dunnett's multiple comparison test as a *post hoc* test for individual differences using GraphPad Prism and a significance level of $p < 0.05$ for all comparisons. Pharmacokinetic data were fitted with standard non-compartmental and one compartment models in Phoenix WinNonlin using default settings and unweighted errors. Transplanted skin graft survivals are shown as Kaplan-Meier survival curves and were compared using the corresponding log-rank (Mantel-Cox) test in GraphPad Prism.

Supplementary Material

Refer to Web version on PubMed Central for supplementary material.

Acknowledgments

This work was supported by a grant from the National Institutes of Health National Institute of Allergy and Infectious Diseases (1R01AI101041, PI: P. Buchwald). We thank Drs. Jodie Johnson and Kari Basso from the Mass Spectrometry Laboratory at the University of Florida for their prompt and professional service.

ABBREVIATIONS USED

AID	activation-induced cytidine deaminase
PPI	protein-protein interaction
T1D	type 1 diabetes

TNF tumor necrosis factor.

References

1. Chen L, Flies DB. Molecular mechanisms of T cell co-stimulation and co-inhibition. Nat. Rev. Immunol. 2013; 13(4):227–242. [PubMed: 23470321]
2. Gao W, Demirci G, Li XC. Negative T cell costimulation and islet tolerance. Diabetes Metab. Res. Rev. 2003; 19(3):179–185. [PubMed: 12789650]
3. Larsen CP, Knechtle SJ, Adams A, Pearson T, Kirk AD. A new look at blockade of T-cell costimulation: a therapeutic strategy for long-term maintenance immunosuppression. Am. J. Transplant. 2006; 6(5 Pt 1):876–883. [PubMed: 16611323]
4. Vincenti F, Luggen M. T cell costimulation: a rational target in the therapeutic armamentarium for autoimmune diseases and transplantation. Annu. Rev. Med. 2007; 58:347–358. [PubMed: 17020493]
5. Weaver TA, Charafeddine AH, Kirk AD. Costimulation blockade: towards clinical application. Front. Biosci. 2008; 13:2120–2139. [PubMed: 17981697]
6. Li XC, Rothstein DM, Sayegh MH. Costimulatory pathways in transplantation: challenges and new developments. Immunol. Rev. 2009; 229(1):271–293. [PubMed: 19426228]
7. Peters AL, Stunz LL, Bishop GA. CD40 and autoimmunity: The dark side of a great activator. Semin. Immunol. 2009; 21(5):293–300. [PubMed: 19595612]
8. Croft M, Benedict CA, Ware CF. Clinical targeting of the TNF and TNFR superfamilies. Nat. Rev. Drug Discov. 2013; 12(2):147–168. [PubMed: 23334208]
9. Schönbeck U, Libby P. The CD40/CD154 receptor/ligand dyad. Cell Mol. Life Sci. 2001; 58(1):4–43. [PubMed: 11229815]
10. An HJ, Kim YJ, Song DH, Park BS, Kim HM, Lee JD, Paik SG, Lee JO, Lee H. Crystallographic and mutational analysis of the CD40-CD154 complex and its implications for receptor activation. J. Biol. Chem. 2011; 286(13):11226–11235. [PubMed: 21285457]
11. Kenyon NS, Chatzipetrou M, Masetti M, Ranuncoli A, Oliveira M, Wagner JL, Kirk AD, Harlan DM, Burkly LC, Ricordi C. Long-term survival and function of intrahepatic islet allografts in rhesus monkeys treated with humanized anti-CD154. Proc. Natl. Acad. Sci. U.S.A. 1999; 96(14): 8132–8137. [PubMed: 10393960]
12. Cardona K, Korbutt GS, Milas Z, Lyon J, Cano J, Jiang W, Bello-Laborn H, Hacquoil B, Strobert E, Gangappa S, Weber CJ, Pearson TC, Rajotte RV, Larsen CP. Long-term survival of neonatal porcine islets in nonhuman primates by targeting costimulation pathways. Nat. Med. 2006; 12(3): 304–306. [PubMed: 16501570]
13. Burkly LC. CD40 pathway blockade as an approach to immunotherapy. Adv. Exp. Med. Biol. 2001; 489:135–152. [PubMed: 11554588]
14. Quezada SA, Jarvinen LZ, Lind EF, Noelle RJ. CD40/CD154 interactions at the interface of tolerance and immunity. Annu. Rev. Immunol. 2004; 22:307–328. [PubMed: 15032580]
15. Elgueta R, Benson MJ, de Vries VC, Wasiuk A, Guo Y, Noelle RJ. Molecular mechanism and function of CD40/CD40L engagement in the immune system. Immunol. Rev. 2009; 229(1):152–172. [PubMed: 19426221]
16. Wagner DH Jr, Vaitaitis G, Sanderson R, Poulin M, Dobbs C, Haskins K. Expression of CD40 identifies a unique pathogenic T cell population in type 1 diabetes. Proc. Natl. Acad. Sci. U.S.A. 2002; 99(6):3782–3787. [PubMed: 11891296]
17. Bour-Jordan H, Salomon BL, Thompson HL, Szot GL, Bernhard MR, Bluestone JA. Costimulation controls diabetes by altering the balance of pathogenic and regulatory T cells. J. Clin. Invest. 2004; 114(7):979–987. [PubMed: 15467837]
18. Baker RL, Mallevaey T, Gapin L, Haskins K. T cells interact with T cells via CD40-CD154 to promote autoimmunity in type 1 diabetes. Eur. J. Immunol. 2012; 42(3):672–680. [PubMed: 22488364]

19. Vaitaitis GM, Olmstead MH, Waid DM, Carter JR, Wagner DH Jr. A CD40-targeted peptide controls and reverses type 1 diabetes in NOD mice. Diabetologia. 2014; 57:2366–2373. [PubMed: 25104468]
20. Foy TM, Aruffo A, Bajorath J, Buhlmann JE, Noelle RJ. Immune regulation by CD40 and its ligand GP39. Annu. Rev. Immunol. 1996; 14:591–617. [PubMed: 8717526]
21. Graf D, Muller S, Korthauer U, van Kooten C, Weise C, Kroczek RA. A soluble form of TRAP (CD40 ligand) is rapidly released after T cell activation. Eur. J. Immunol. 1995; 25(6):1749–1754. [PubMed: 7615003]
22. Mazzei GJ, Edgerton MD, Losberger C, Lecoanet-Henchoz S, Graber P, Durandy A, Gauchat JF, Bernard A, Allet B, Bonnefoy JY. Recombinant soluble trimeric CD40 ligand is biologically active. J. Biol. Chem. 1995; 270(13):7025–7028. [PubMed: 7706236]
23. Thusberg J, Vihinen M. The structural basis of hyper IgM deficiency - CD40L mutations. Protein Eng. Des. Sel. 2007; 20(3):133–141. [PubMed: 17307885]
24. Pamukcu B, Lip GY, Snezhitskiy V, Shantsila E. The CD40-CD40L system in cardiovascular disease. Ann. Med. 2011; 43(5):331–340. [PubMed: 21244217]
25. Senhaji N, Kojok K, Darif Y, Fadainia C, Zaid Y. The contribution of CD40/CD40L axis in inflammatory bowel disease: an update. Front. Immunol. 2015; 6:529. [PubMed: 26528290]
26. Wolf D, Jehle F, Michel NA, Bukosza EN, Rivera J, Chen YC, Hoppe N, Dufner B, Rodriguez AO, Colberg C, Nieto L, Rupprecht B, Wiedemann A, Schulte L, Peikert A, Bassler N, Lozhkin A, Hergeth SP, Stachon P, Hilgendorf I, Willecke F, von Zur Muhlen C, von Elverfeldt D, Binder CJ, Aichele P, Varo N, Febbraio MA, Libby P, Bode C, Peter K, Zirlik A. Coinhibitory suppression of T cell activation by CD40 protects against obesity and adipose tissue inflammation in mice. Circulation. 2014; 129(23):2414–2425. [PubMed: 24664276]
27. Bagnati M, Ogunkolade BW, Marshall C, Tucci C, Hanna K, Jones TA, Bugliani M, Nedjai B, Caton PW, Kieswich J, Yaqoob MM, Ball GR, Marchetti P, Hitman GA, Turner MD. Glucolipotoxicity initiates pancreatic β-cell death through TNFR5/CD40-mediated STAT1 and NF-κB activation. Cell Death Dis. 2016; 7(8):e2329. [PubMed: 27512950]
28. Kawai T, Andrews D, Colvin RB, Sachs DH, Cosimi AB. Thromboembolic complications after treatment with monoclonal antibody against CD40 ligand. Nat. Med. 2000; 6(2):114.
29. Boumpas DT, Furie R, Manzi S, Illei GG, Wallace DJ, Balow JE, Vaishnaw A. Group, B. G. L. N. T. A short course of BG9588 (anti-CD40 ligand antibody) improves serologic activity and decreases hematuria in patients with proliferative lupus glomerulonephritis. Arthritis Rheum. 2003; 48(3):719–727. [PubMed: 12632425]
30. Koyama I, Kawai T, Andrews D, Boskovic S, Nadazdin O, Wee SL, Sogawa H, Wu DL, Smith RN, Colvin RB, Sachs DH, Cosimi AB. Thrombophilia associated with anti-CD154 monoclonal antibody treatment and its prophylaxis in nonhuman primates. Transplantation. 2004; 77(3):460–462. [PubMed: 14966427]
31. Roth GA, Zuckermann A, Klepetko W, Wolner E, Ankersmit HJ, Moser B, Volf I. Thrombophilia associated with anti-CD154 monoclonal antibody treatment and its prophylaxis in nonhuman primates. Transplantation. 2004; 78(8):1238–1239. [PubMed: 15502729]
32. Couzin J. Drug discovery. Magnificent obsession. Science. 2005; 307(5716):1712–1715. [PubMed: 15774740]
33. Mirabet M, Barrabes JA, Quiroga A, Garcia-Dorado D. Platelet pro-aggregatory effects of CD40L monoclonal antibody. Mol. Immunol. 2008; 45(4):937–944. [PubMed: 17959249]
34. Xie JH, Yamniuk AP, Borowski V, Kuhn R, Susulic V, Rex-Rabe S, Yang X, Zhou X, Zhang Y, Gillooly K, Brosius R, Ravishankar R, Waggie K, Mink K, Price L, Rehfuss R, Tamura J, An Y, Cheng L, Abramczyk B, Ignatovich O, Drew P, Grant S, Bryson JW, Suchard S, Salter-Cid L, Nadler S, Suri A. Engineering of a novel anti-CD40L domain antibody for treatment of autoimmune diseases. J. Immunol. 2014; 192(9):4083–4092. [PubMed: 24670803]
35. Kim SC, Wakwe W, Higginbotham LB, Mathews DV, Breeden CP, Stephenson AC, Jenkins J, Strobert E, Price K, Price L, Kuhn R, Wang H, Yamniuk A, Suchard S, Farris AB 3rd, Pearson TC, Larsen CP, Ford ML, Suri A, Nadler S, Adams AB. Fc-Silent anti-CD154 domain antibody effectively prevents nonhuman primate renal allograft rejection. Am. J. Transplant. 2017; 17(5): 1182–1192. [PubMed: 28097811]

36. Leader B, Baca QJ, Golan DE. Protein therapeutics: a summary and pharmacological classification. Nat. Rev. Drug Discov. 2008; 7(1):21–39. [PubMed: 18097458]
37. Downing NS, Shah ND, Aminawung JA, Pease AM, Zeitoun JD, Krumholz HM, Ross JS. Postmarket safety events among novel therapeutics approved by the US Food and Drug Administration between 2001 and 2010. J. Am. Med. Assoc. (JAMA). 2017; 317(18):1854–1863.
38. Sathish JG, Sethu S, Bielsky MC, de Haan L, French NS, Govindappa K, Green J, Griffiths CE, Holgate S, Jones D, Kimber I, Moggs J, Naisbitt DJ, Pirmohamed M, Reichmann G, Sims J, Subramanyam M, Todd MD, Van Der Laan JW, Weaver RJ, Park BK. Challenges and approaches for the development of safer immunomodulatory biologics. Nat. Rev. Drug Discov. 2013; 12(4): 306–324. [PubMed: 23535934]
39. Deambrosis I, Lamorte S, Giaretta F, Tei L, Biancone L, Bussolati B, Camussi G. Inhibition of CD40-CD154 costimulatory pathway by a cyclic peptide targeting CD154. J. Mol. Med. 2009; 87(2):181–197. [PubMed: 18985310]
40. André P, Prasad KS, Denis CV, He M, Papalia JM, Hynes RO, Phillips DR, Wagner DD. CD40L stabilizes arterial thrombi by a β3 integrin-dependent mechanism. Nat. Med. 2002; 8(3):247–252. [PubMed: 11875495]
41. Wolf D, Hohmann JD, Wiedemann A, Bledzka K, Blankenbach H, Marchini T, Gutte K, Zeschky K, Bassler N, Hoppe N, Rodriguez AO, Herr N, Hilgendorf I, Stachon P, Willecke F, Duerschmied D, von zur Muhlen C, Soloviev DA, Zhang L, Bode C, Plow EF, Libby P, Peter K, Zirlik A. Binding of CD40L to Mac-1's I-domain involves the EQLKKSKTL motif and mediates leukocyte recruitment and atherosclerosis--but does not affect immunity and thrombosis in mice. Circ. Res. 2011; 109(11):1269–1279. [PubMed: 21998326]
42. Giannoukakis N, Phillips B, Trucco M. Toward a cure for type 1 diabetes mellitus: diabetes-suppressive dendritic cells and beyond. Pediatr. Diabetes. 2008; 9(3 Pt 2):4–13. [PubMed: 18540865]
43. Skyler JS, Ricordi C. Stopping type 1 diabetes: attempts to prevent or cure type 1 diabetes in man. Diabetes. 2011; 60(1):1–8. [PubMed: 21193733]
44. von Herrath M, Peakman M, Roep B. Progress in immune-based therapies for type 1 diabetes. Clin. Exp. Immunol. 2013; 172(2):186–202. [PubMed: 23574316]
45. Lernmark Å, Larsson HE. Immune therapy in type 1 diabetes mellitus. Nat. Rev. Endocrinol. 2013; 9(2):92–103. [PubMed: 23296174]
46. Schneider DA, Kretowicz AM, von Herrath MG. Emerging immune therapies in type 1 diabetes and pancreatic islet transplantation. Diabetes. Obes. Metab. 2013; 15(7):581–592. [PubMed: 23194064]
47. Skyler JS. Primary and secondary prevention of Type 1 diabetes. Diabet. Med. 2013; 30(2):161–169. [PubMed: 23231526]
48. Skyler JS. Prevention and reversal of type 1 diabetes - past challenges and future opportunities. Diabetes Care. 2015; 38(6):997–1007. [PubMed: 25998292]
49. Donath MY, Hess C, Palmer E. What is the role of autoimmunity in type 1 diabetes? A clinical perspective. Diabetologia. 2014; 57(4):653–655. [PubMed: 24389751]
50. Lo Conte L, Chothia C, Janin J. The atomic structure of protein-protein recognition sites. J. Mol. Biol. 1999; 285(5):2177–2198. [PubMed: 9925793]
51. Wells JA, McClendon CL. Reaching for high-hanging fruit in drug discovery at protein-protein interfaces. Nature. 2007; 450(7172):1001–1009. [PubMed: 18075579]
52. Berg T. Modulation of protein-protein interactions with small organic molecules. Angew. Chem. Int. Ed. Engl. 2003; 42(22):2462–2481. [PubMed: 12800163]
53. Arkin MR, Wells JA. Small-molecule inhibitors of protein-protein interactions: progressing towards the dream. Nat. Rev. Drug Discov. 2004; 3(4):301–317. [PubMed: 15060526]
54. Fry DC. Protein-protein interactions as targets for small molecule drug discovery. Biopolymers. 2006; 84(6):535–552. [PubMed: 17009316]
55. Whitty A, Kumaravel G. Between a rock and a hard place? Nat. Chem. Biol. 2006; 2(3):112–118. [PubMed: 16484997]
56. Wilson AJ. Inhibition of protein-protein interactions using designed molecules. Chem. Soc. Rev. 2009; 38(12):3289–3300. [PubMed: 20449049]

57. Buchwald P. Small-molecule protein-protein interaction inhibitors: therapeutic potential in light of molecular size, chemical space, and ligand binding efficiency considerations. IUBMB Life. 2010; 62(10):724–731. [PubMed: 20979208]
58. Mullard A. Protein-protein interaction inhibitors get into the groove. Nat. Rev. Drug Discov. 2012; 11(3):173–175. [PubMed: 22378255]
59. Arkin MR, Tang Y, Wells JA. Small-molecule inhibitors of protein-protein interactions: Progressing toward the reality. Chem. Biol. 2014; 21(9):1102–1114. [PubMed: 25237857]
60. Milroy LG, Grossmann TN, Hennig S, Brunsveld L, Ottmann C. Modulators of protein-protein interactions. Chem. Rev. 2014; 114(9):4695–4748. [PubMed: 24735440]
61. Laraia L, McKenzie G, Spring DR, Venkitaraman AR, Huggins DJ. Overcoming chemical, biological, and computational challenges in the development of inhibitors targeting protein-protein interactions. Chem. Biol. 2015; 22(6):689–703. [PubMed: 26091166]
62. Song Y, Buchwald P. TNF superfamily protein-protein interactions: feasibility of small-molecule modulation. Curr. Drug. Targets. 2015; 16:393–408. [PubMed: 25706111]
63. Scott DE, Bayly AR, Abell C, Skidmore J. Small molecules, big targets: drug discovery faces the protein-protein interaction challenge. Nat. Rev. Drug Discov. 2016; 15(8):533–550. [PubMed: 27050677]
64. Souers AJ, Leverson JD, Boghaert ER, Ackler SL, Catron ND, Chen J, Dayton BD, Ding H, Enschede SH, Fairbrother WJ, Huang DC, Hymowitz SG, Jin S, Khaw SL, Kovar PJ, Lam LT, Lee J, Maecker HL, Marsh KC, Mason KD, Mitten MJ, Nimmer PM, Oleksijew A, Park CH, Park CM, Phillips DC, Roberts AW, Sampath D, Seymour JF, Smith ML, Sullivan GM, Tahir SK, Tse C, Wendt MD, Xiao Y, Xue JC, Zhang H, Humerickhouse RA, Rosenberg SH, Elmore SW. ABT-199, a potent and selective BCL-2 inhibitor, achieves antitumor activity while sparing platelets. Nat. Med. 2013; 19(2):202–208. [PubMed: 23291630]
65. Mullard A. Pioneering apoptosis-targeted cancer drug poised for FDA approval. Nat. Rev. Drug Discov. 2016; 15(3):147–149. [PubMed: 26931080]
66. Gadek TR, Burdick DJ, McDowell RS, Stanley MS, Marsters JC Jr, Paris KJ, Oare DA, Reynolds ME, Ladner C, Zioncheck KA, Lee WP, Gribling P, Dennis MS, Skelton NJ, Tumas DB, Clark KR, Keating SM, Beresini MH, Tilley JW, Presta LG, Bodary SC. Generation of an LFA-1 antagonist by the transfer of the ICAM-1 immunoregulatory epitope to a small molecule. Science. 2002; 295(5557):1086–1089. [PubMed: 11834839]
67. Margolles-Clark E, Jacques-Silva MC, Ganesan L, Umland O, Kenyon NS, Ricordi C, Berggren P-O, Buchwald P. Suramin inhibits the CD40–CD154 costimulatory interaction: a possible mechanism for immuno effects. Biochem. Pharmacol. 2009; 77(7):1236–1245. [PubMed: 19283894]
68. Margolles-Clark E, Umland O, Kenyon NS, Ricordi C, Buchwald P. Small molecule costimulatory blockade: organic dye inhibitors of the CD40-CD154 interaction. J. Mol. Med. 2009; 87(11): 1133–1143. [PubMed: 19707732]
69. Margolles-Clark E, Kenyon NS, Ricordi C, Buchwald P. Effective and specific inhibition of the CD40-CD154 costimulatory interaction by a naphthalenesulphonic acid derivative. Chem. Biol. Drug Des. 2010; 76(4):305–313. [PubMed: 20636329]
70. Song Y, Margolles-Clark E, Bayer A, Buchwald P. Small-molecule modulators of the OX40–OX40L costimulatory protein–protein interaction. Br. J. Pharmacol. 2014; 171(21):4955–4969. [PubMed: 24930776]
71. Ganesan L, Margolles-Clark E, Song Y, Buchwald P. The food colorant erythrosine is a promiscuous protein-protein interaction inhibitor. Biochem. Pharmacol. 2011; 81(6):810–818. [PubMed: 21219880]
72. Ganesan L, Buchwald P. The promiscuous protein binding ability of erythrosine B studied by metachromasy (metachromasia). J. Mol. Recognit. 2013; 26(4):181–189. [PubMed: 23456742]
73. Buchwald, P. Inhibitors of TNF superfamily costimulatory interactions and methods for uses of the same. International Patent Application no. PCT/US. 16/66821. Dec 15. 2016
74. Venkatraj M, Messagie J, Joossens J, Lambeir AM, Haemers A, Van der Veken P, Augustyns K. Synthesis and evaluation of non-basic inhibitors of urokinase-type plasminogen activator (uPA). Bioorg. Med. Chem. 2012; 20(4):1557–1568. [PubMed: 22285569]

75. Kassack MU, Braun K, Ganso M, Ullmann H, Nickel P, Boing B, Muller G, Lambrecht G. Structure-activity relationships of analogues of NF449 confirm NF449 as the most potent and selective known P2X1 receptor antagonist. Eur. J. Med. Chem. 2004; 39(4):345–357. [PubMed: 15072843]
76. Roterman I, No KT, Piekarska B, Kaszuba J, Pawlicki R, Rybarska J, Konieczny L. Bis azo dyes - studies on the mechanism of complex formation with IgG modulated by heating or antigen binding. J. Physiol. Pharmacol. 1993; 44(3):213–232. [PubMed: 8241524]
77. Stopa B, Gorny M, Konieczny L, Piekarska B, Rybarska J, Skowronek M, Roterman I. Supramolecular ligands: monomer structure and protein ligation capability. Biochimie. 1998; 80(12):963–968. [PubMed: 9924974]
78. McGovern SL, Caselli E, Grigorieff N, Shoichet BK. A common mechanism underlying promiscuous inhibitors from virtual and high-throughput screening. J. Med. Chem. 2002; 45:1712–1722. [PubMed: 11931626]
79. Shoichet BK. Screening in a spirit haunted world. Drug Discov. Today. 2006; 11(13–14):607–615. [PubMed: 16793529]
80. Aldrich C, Bertozzi C, Georg GI, Kiessling L, Lindsley C, Liotta D, Merz KM Jr, Schepartz A, Wang S. The ecstasy and agony of assay interference compounds. J. Med. Chem. 2017; 60(6): 2165–2168. [PubMed: 28244745]
81. Feng BY, Shoichet BK. A detergent-based assay for the detection of promiscuous inhibitors. Nat. Protoc. 2006; 1(2):550–553. [PubMed: 17191086]
82. Smith, CG., O'Donnell, JT. The Process of New Drug Discovery and Development. 2. Informa Healthcare; New York: 2007. p. 657
83. Bodor, N., Buchwald, P. Retrometabolic Drug Design and Targeting. 1. Wiley; Hoboken, NJ: 2012. p. 418
84. Miyazawa M, Ito Y, Kosaka N, Nukada Y, Sakaguchi H, Suzuki H, Nishiyama N. Role of TNF-alpha and extracellular ATP in THP-1 cell activation following allergen exposure. J. Toxicol. Sci. 2008; 33(1):71–83. [PubMed: 18303186]
85. Zan H, Casali P. Regulation of Aicda expression and AID activity. Autoimmunity. 2013; 46(2):83–101. [PubMed: 23181381]
86. Dedeoglu F, Horwitz B, Chaudhuri J, Alt FW, Geha RS. Induction of activation-induced cytidine deaminase gene expression by IL-4 and CD40 ligation is dependent on STAT6 and NFκB. Int. Immunol. 2004; 16(3):395–404. [PubMed: 14978013]
87. Pinelli DF, Wagener ME, Liu D, Yamniuk A, Tamura J, Grant S, Larsen CP, Suri A, Nadler SG, Ford ML. An anti-CD154 domain antibody prolongs graft survival and induces Foxp3(+) iTreg in the absence and presence of CTLA-4 Ig. Am. J. Transplant. 2013; 13(11):3021–3030. [PubMed: 24007441]
88. Monk NJ, Hargreaves RE, Simpson E, Dyson JP, Jurcevic S. Transplant tolerance: models, concepts and facts. J. Mol. Med. 2006; 84(4):295–304. [PubMed: 16501935]
89. Fournel S, Wieckowski S, Sun W, Trouche N, Dumortier H, Bianco A, Chaloin O, Habib M, Peter JC, Schneider P, Vray B, Toes RE, Offringa R, Melief CJ, Hoebeke J, Guichard G. C_3-symmetric peptide scaffolds are functional mimetics of trimeric CD40L. Nat. Chem. Biol. 2005; 1(7):377–382. [PubMed: 16370373]
90. Allen SD, Rawale SV, Whitacre CC, Kaumaya PT. Therapeutic peptidomimetic strategies for autoimmune diseases: costimulation blockade. J. Pept. Res. 2005; 65(6):591–604. [PubMed: 15885118]
91. Kitagawa M, Goto D, Mamura M, Matsumoto I, Ito S, Tsutsumi A, Sumida T. Identification of three novel peptides that inhibit CD40-CD154 interaction. Mod. Rheumatol. 2005; 15(6):423–426. [PubMed: 17029106]
92. Silvian LF, Friedman JE, Strauch K, Cachero TG, Day ES, Qian F, Cunningham B, Fung A, Sun L, Shipps GW, Su L, Zheng Z, Kumaravel G, Whitty A. Small molecule inhibition of the TNF family cytokine CD40 ligand through a subunit fracture mechanism. ACS Chem. Biol. 2011; 6(6):636–647. [PubMed: 21417339]
93. Hajduk PJ, Bures M, Praestgaard J, Fesik SW. Privileged molecules for protein binding identified from NMR-based screening. J. Med. Chem. 2000; 43(18):3443–3447. [PubMed: 10978192]

94. Yin H, Hamilton AD. Strategies for targeting protein-protein interactions with synthetic agents. Angew. Chem. Int. Ed. Engl. 2005; 44(27):4130–4163. [PubMed: 15954154]

95. Che Y, Brooks BR, Marshall GR. Development of small molecules designed to modulate protein-protein interactions. J. Comput. Aided Mol. Des. 2006; 20(2):109–130. [PubMed: 16622794]

96. Khan, MM. Immunopharmacology. Springer; New York: 2008. p. 266

97. Hershberger SJ, Lee SG, Chmielewski J. Scaffolds for blocking protein-protein interactions. Curr. Top. Med. Chem. 2007; 7(10):928–942. [PubMed: 17508924]

98. Levine WG. Metabolism of azo dyes: implication for detoxication and activation. Drug Metab. Rev. 1991; 23(3–4):253–309. [PubMed: 1935573]

99. Feng J, Cerniglia CE, Chen H. Toxicological significance of azo dye metabolism by human intestinal microbiota. Front. Biosci. 2012; 4:568–586.

100. Lipinski CA, Lombardo F, Dominy BW, Feeney PJ. Experimental and computational approaches to estimate solubility and permeability in drug discovery and development setting. Adv. Drug Deliv. Rev. 1997; 23:3–25.

101. Hopkins AL, Groom CR, Alex A. Ligand efficiency: a useful metric for lead selection. Drug Discov. Today. 2004; 9(10):430–431. [PubMed: 15109945]

102. Hajduk PJ. Fragment-based drug design: how big is too big? J. Med. Chem. 2006; 49(24):6972–6976. [PubMed: 17125250]

103. Reynolds CH, Bembenek SD, Tounge BA. The role of molecular size in ligand efficiency. Bioorg. Med. Chem. Lett. 2007; 17(15):4258–4261. [PubMed: 17532632]

104. Buchwald P. Glucocorticoid receptor binding: a biphasic dependence on molecular size as revealed by the bilinear LinBiExp model. Steroids. 2008; 73(2):193–208. [PubMed: 18022656]

105. Adachi Y, Nakagawa H, Matsuo K, Suzuki T, Miyata N. Photoactivatable HNO-releasing compounds using the retro-Diels-Alder reaction. Chem. Commun. 2008; (41):5149–5151.

106. Still WC, Kahn M, Mitra A. Rapid chromatographic technique for preparative separations with moderate resolution. J. Org. Chem. 1978; 43(14):2923–2925.

107. Yadagiri B, Holagunda UD, Bantu R, Nagarapu L, Guguloth V, Polepally S, Jain N. Rational design, synthesis and anti-proliferative evaluation of novel benzosuberone tethered with hydrazide-hydrazones. Bioorg. Med. Chem. Lett. 2014; 24(21):5041–5044. [PubMed: 25264072]

108. Cechin SR, Buchwald P. Effects of representative glucocorticoids on TNFα- and CD40L-induced NF-κB activation in sensor cells. Steroids. 2014; 85:36–43. [PubMed: 24747770]

109. Suter SE, Gouthro TA, McSweeney PA, Nash RA, Haskins ME, Felsburg PJ, Henthorn PS. Optimized transduction of canine paediatric CD34(+) cells using an MSCV-based bicistronic vector. Vet. Res. Commun. 2006; 30(8):881–901. [PubMed: 17139538]

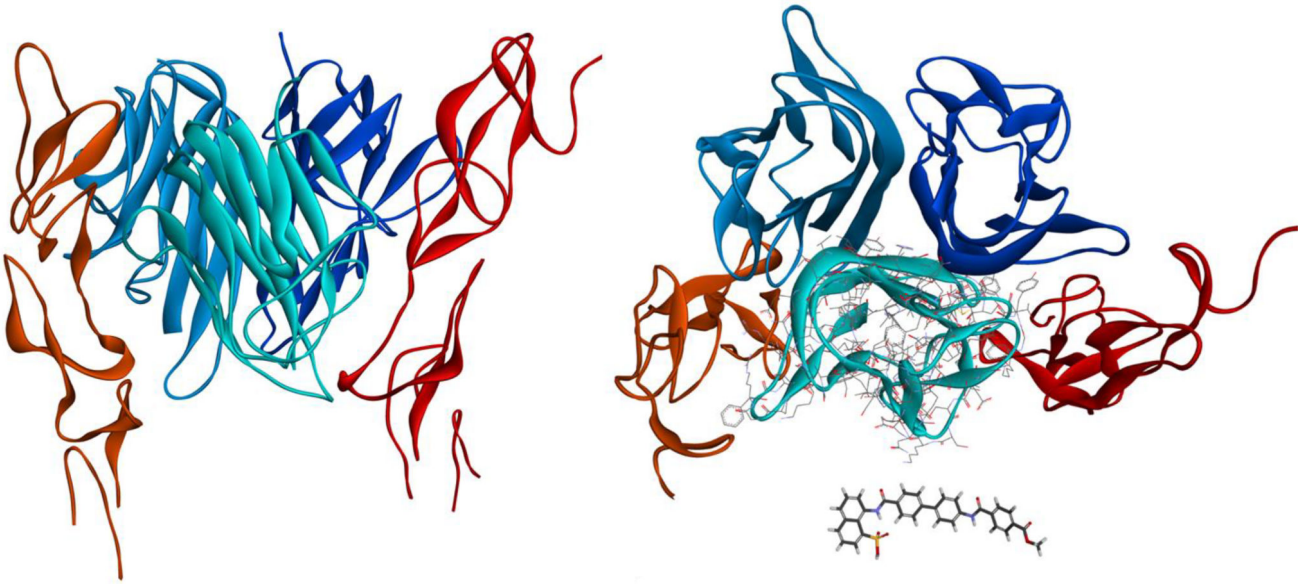

Figure 1.

The interacting trimeric structure of human CD40–CD40L shown from two different perspectives: a side view (left) and a 90°-rotated top view (right). CD40L and CD40 are shown in blue and red hues, respectively using crystal structure of the complex (PDB ID 3QD6[10], which is lacking one of the CD40 monomers). For size comparison, side chains are shown on one of CD40L monomers and our present small molecule of interest (**10**) is included as a separate stick structure.

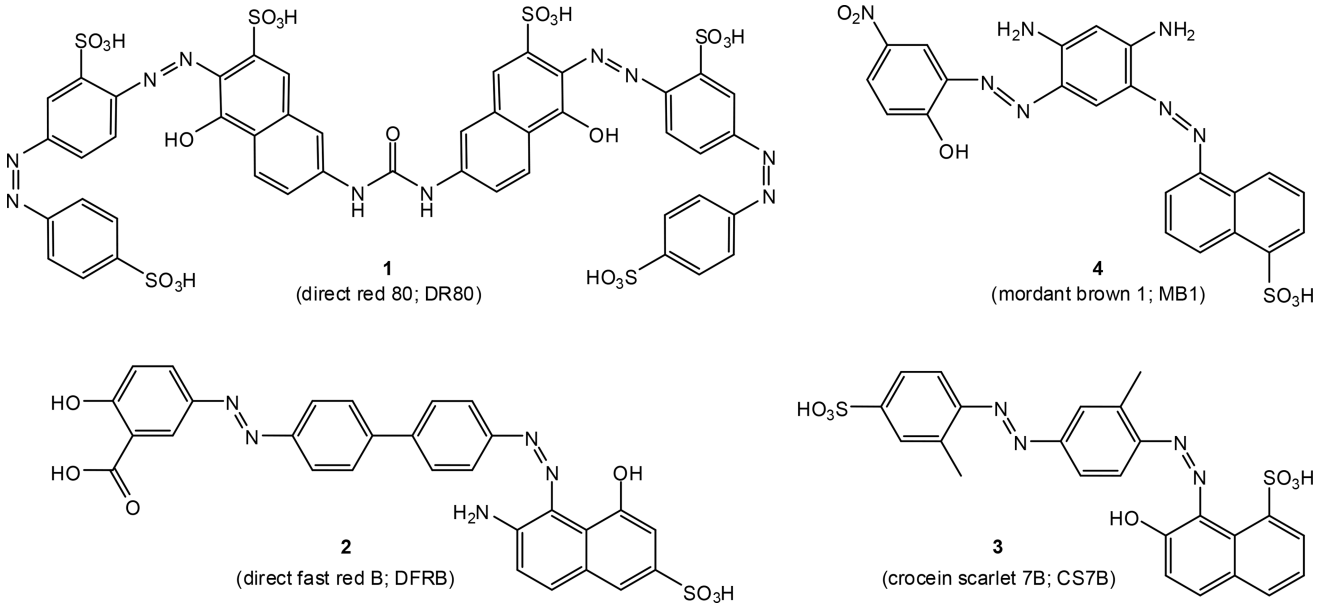

Figure 2.

Organic dye compounds that we have shown previously to inhibit the CD40–CD40L PPI (**1**–**4**)[68, 69] and that served as the starting point for the present study.

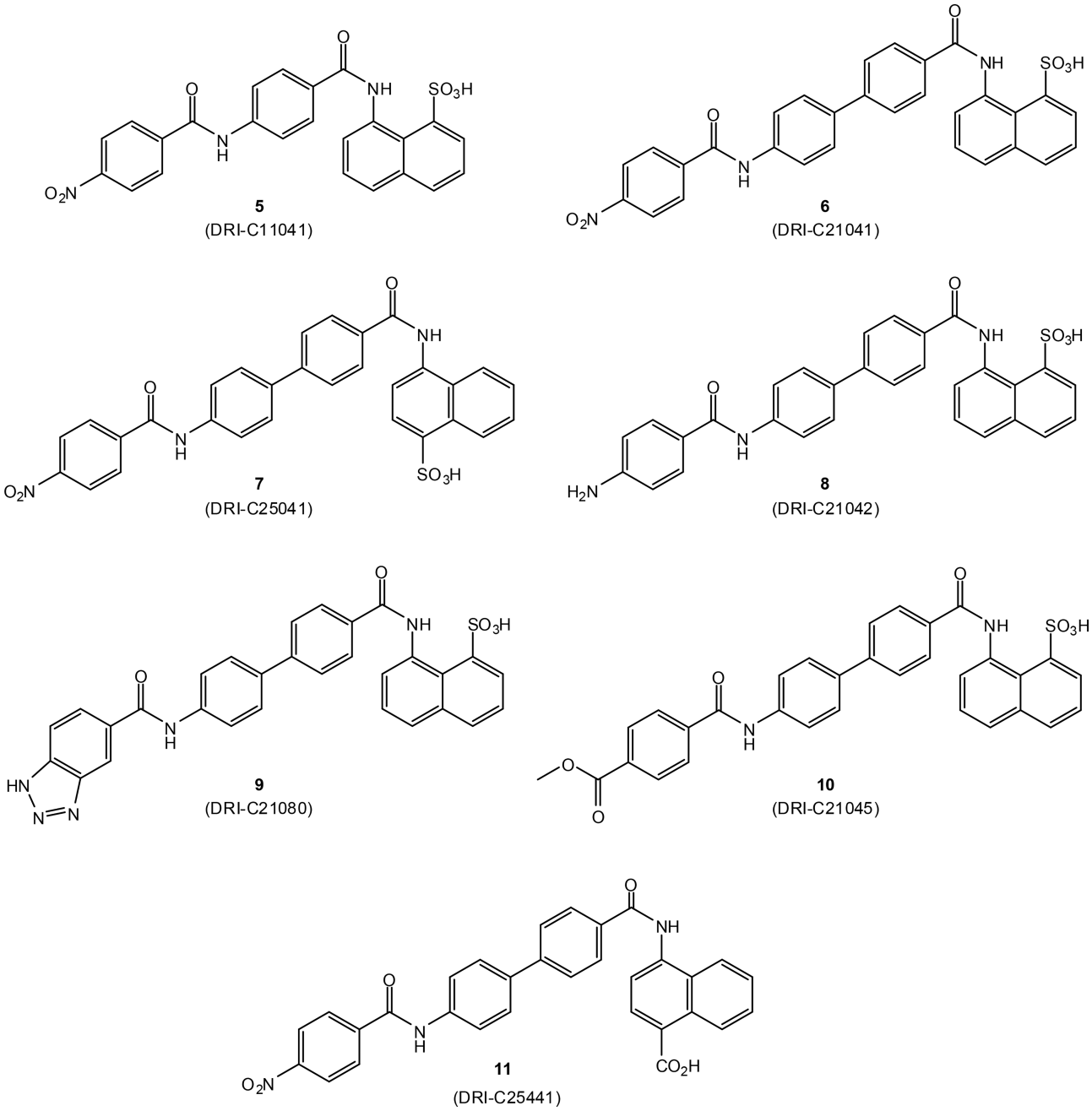

Figure 3.
Structures of compounds **5**–**11** synthesized and investigated in the present study.

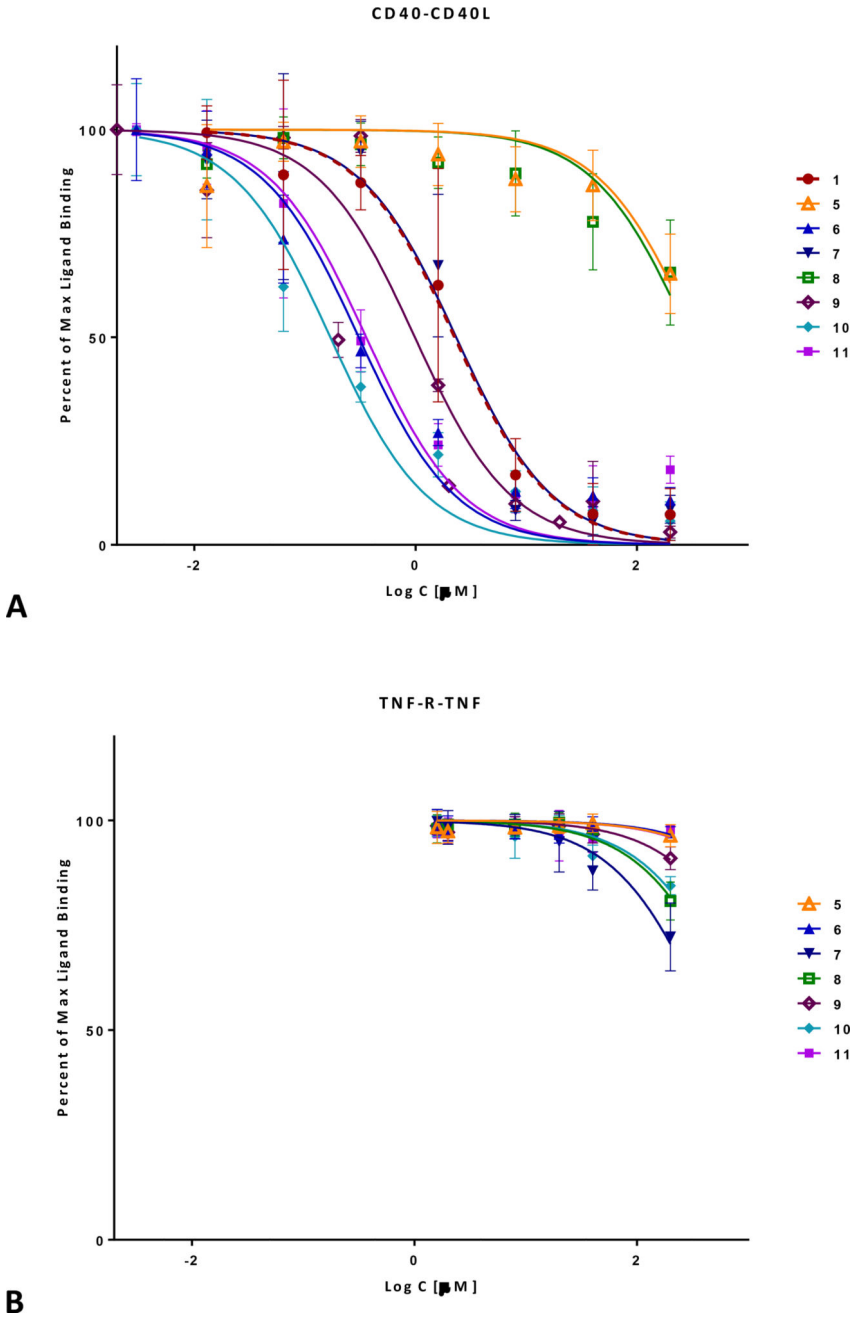

Figure 4.

Concentration-dependent inhibition of the human CD40–CD40L interaction (**A**) and lack of similar inhibition for the human TNF-R–TNFα interaction (**B**) by compounds **5**–**11** (Table 1) quantified using a cell-free ELISA-type assay and fitted with standard binding curves. Our previously identified organic dye inhibitor **1** is included as control. Data are average ± SD (normalized to percent binding) for $n = 3$ independent experiments with triplicates for each condition.

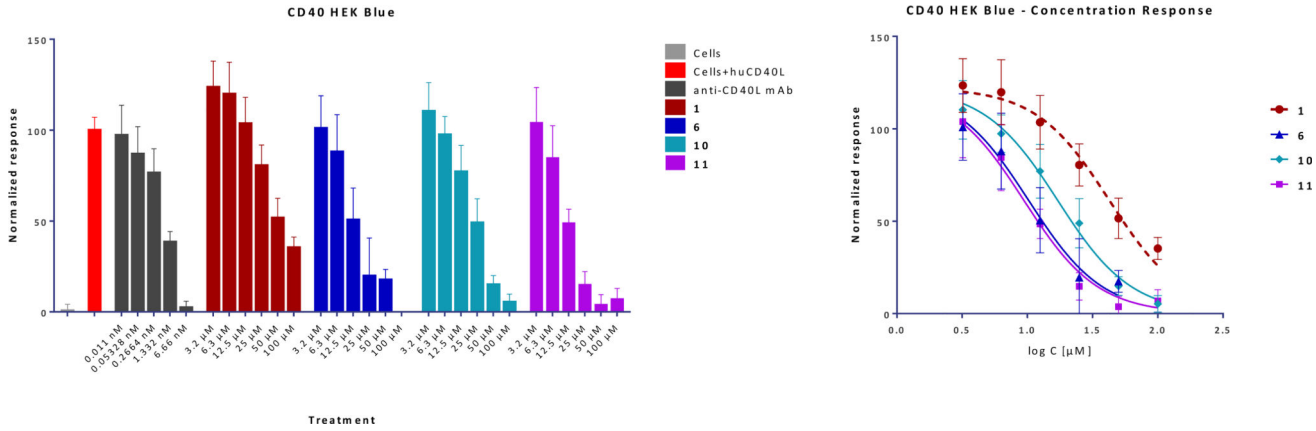

Figure 5.

Concentration-dependent inhibition of CD40L (20 ng/mL) induced NF-κB activation in CD40 sensor cells by **6**, **10**, and **11** with an anti-CD40L antibody (mAb) as positive control. Data are average ± SD (normalized to CD40L-activated cells alone) for $n = 4$ independent experiments with duplicates for each condition. Figure on right shows the concentration response on a classic semi-log scale.

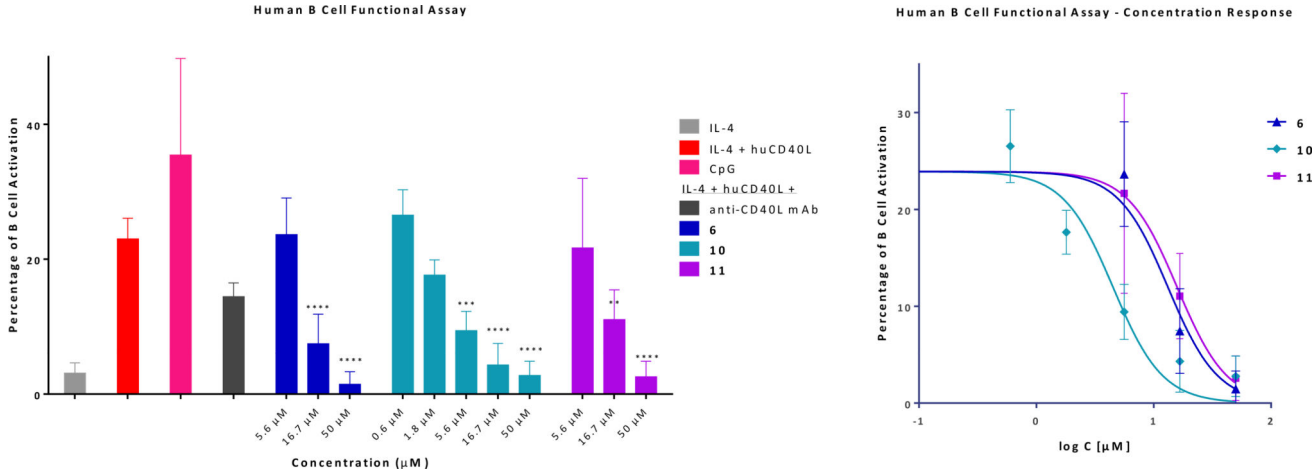

Figure 6.

Concentration-dependent inhibition of CD40L-induced human B-cell function (AID activation quantified via a fluorescent marker detected by flow cytometry) by selected new compounds **6**, **10**, and **11** assessed in a flow cytometry experiment with an anti-CD40L antibody (mAb; 33.3 nM) as positive control. B cells transfected with a lentiviral construct containing the promoter and enhancer region of aicda fused to the reporter Ds-Red were stimulated with IL-4 (0.2 μg/mL) and CD40L (0.2 μg/mL), and the regulation of AID expression through CD40–CD40L signaling under the different conditions was evaluated by Ds-Red level assessed via flow cytometry. Data are average ± SD for three independent experiments and were analyzed by one-way ANOVA followed by Dunnett's multiple comparison test, $^{*}p < 0.05$, $^{**}p < 0.01$, $^{****}p < 0.0001$. Figure on right shows the concentration response on a classic semi-log scale.

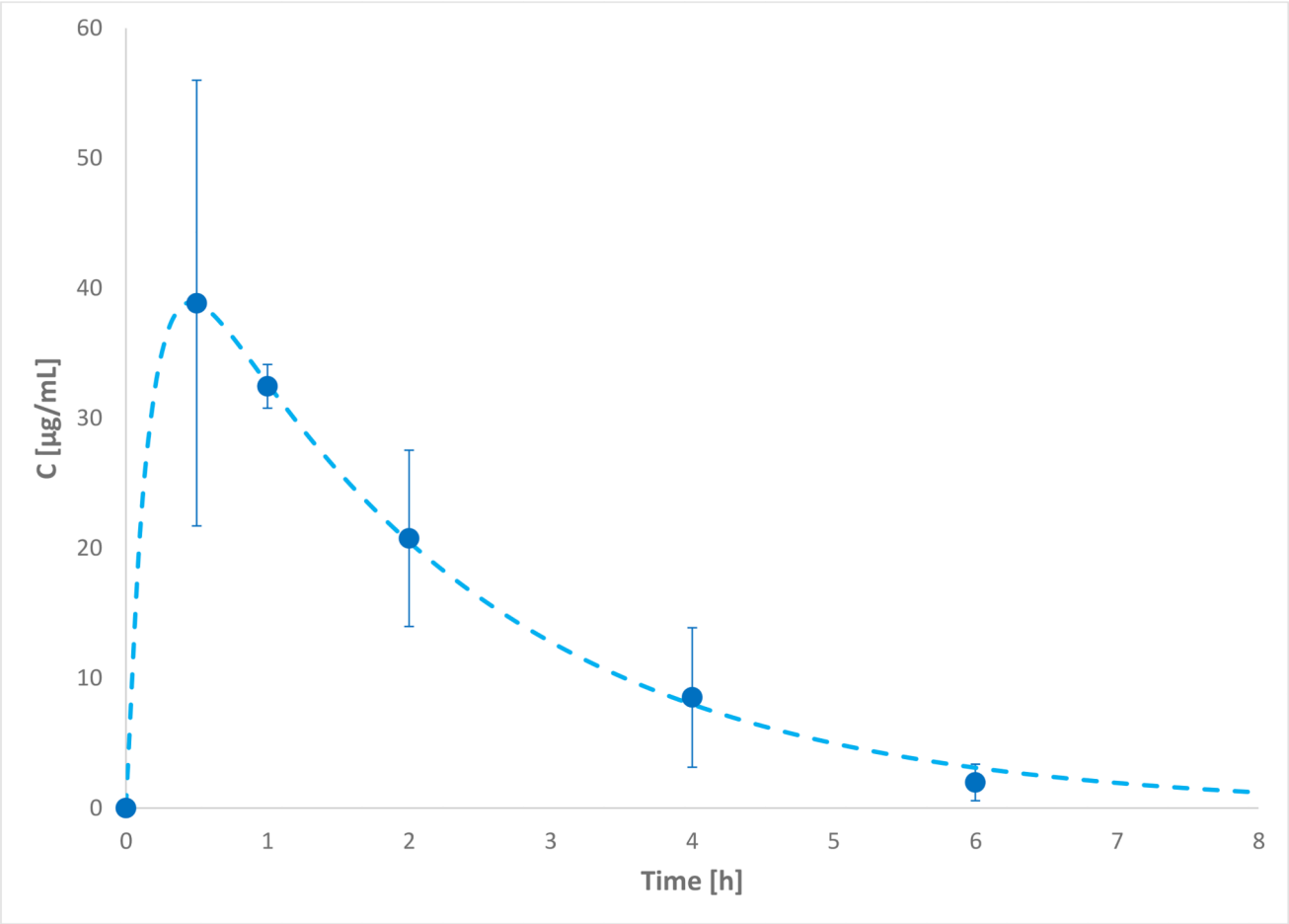

Figure 7.

Pharmacokinetic evaluation in mouse: concentration-time profile of **10** in plasma following a single dose (1.6 mg/mouse, s.c.). Experimental data (average ± SD, $n = 4$; blue symbols) are shown fitted with a standard one compartment, first order absorption, first order elimination pharmacokinetic (PK) model (dotted blue line).

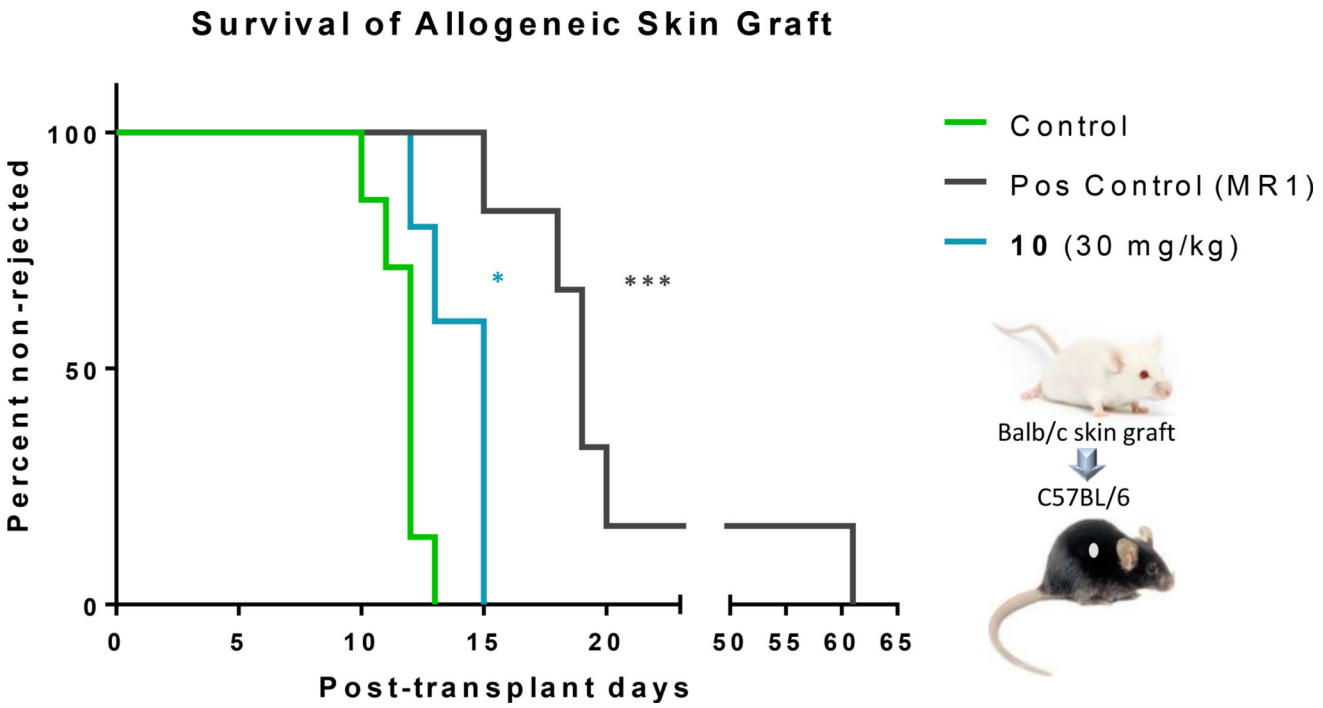

Figure 8.

Prolongation of skin allograft by compound **10**. C57BL6 mice were transplanted with Balb/c skin grafts and treated with 250 μg of CTLA4-Ig (days 0, 2, 4, and 6) plus either CD40L antibody (MR-1; 250 μg; days 0, 2, 4, and 6) or compound **10** (30 mg/kg; daily, s.c. in 20% HPβCD) following the protocol from[87]. Data are with a total of 5–8 mice per group. $^{*}p < 0.05$, $^{***}p < 0.001$ compared to CTLA4-Ig alone using log-rank (Mantel-Cox) test.

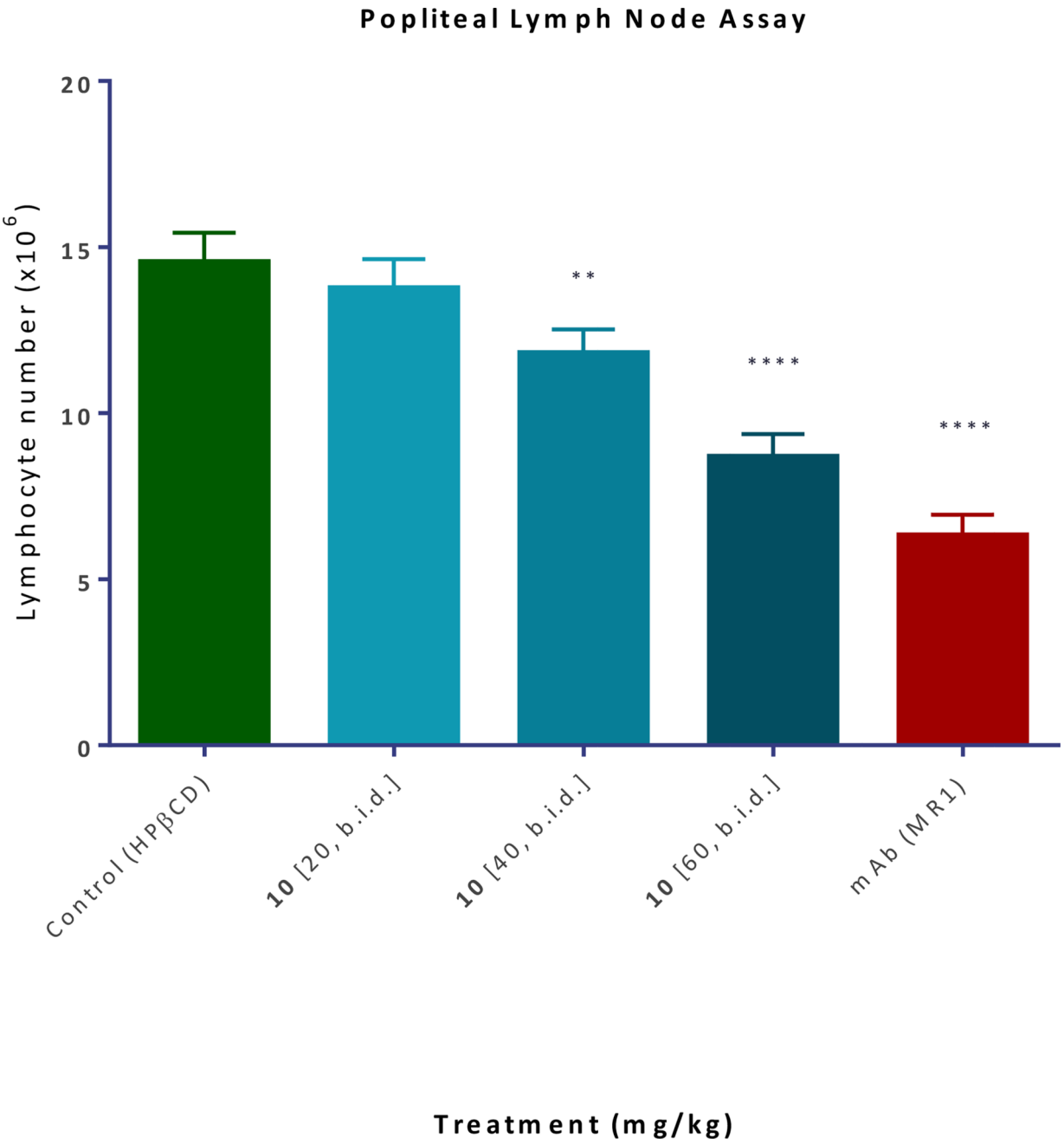

Figure 9.

Inhibition of alloantigen-induced T cell response in a draining lymph node. Balb/c mice received a footpad injection of splenocytes isolated from DBA-2 mice and were treated with CD40L antibody (MR-1; 20 mg/kg, day −1 and 0) or compound **10** (20–60 mg/kg, b.i.d. from −1 to 3, s.c. in 20% HPβCD). The draining popliteal nodes (DLNs) were collected 3 days after the alloantigen challenge and DLN cells were counted[34]. Data are shown as mean ± SD (n = 3–4). Significant differences compared to vehicle-treated controls are indicated by asterisk ($^{**}p < 0.01$, $^{****}p < 0.0001$; one-way ANOVA followed by Dunnett's multiple comparison test).

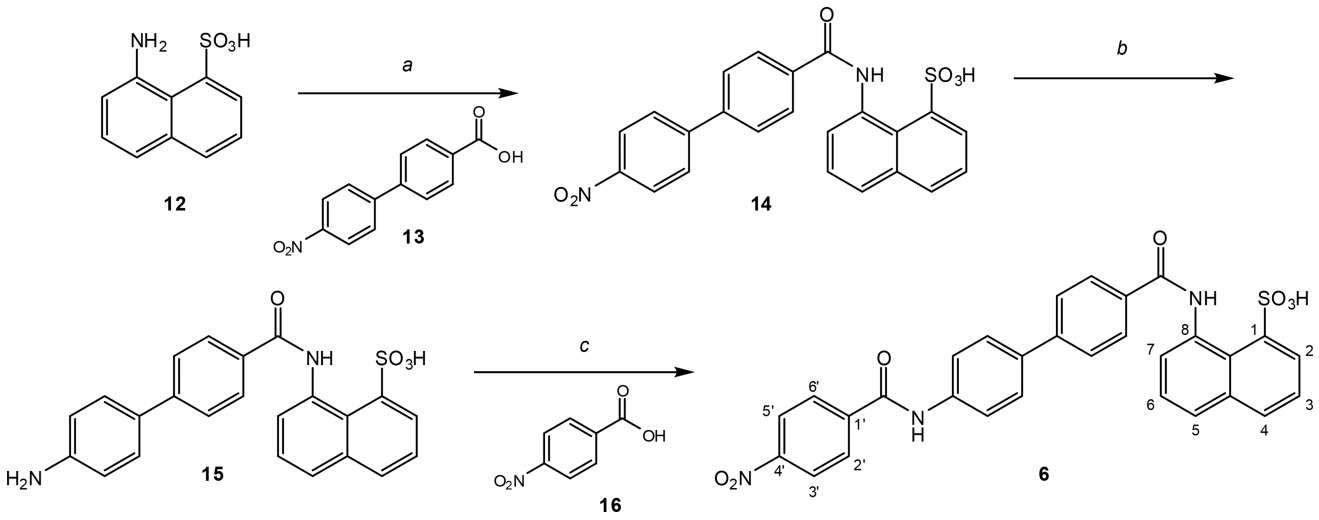

Scheme 1.

General synthetic scheme of the new compounds investigated here illustrated for the case of compound **6**. The general coupling procedure used (*a* and *c*) was similar for all compounds. Reagents and conditions: (*a*) HCTU, Et_3N, DMF, 0°C to RT, 24 h, 65%; (*b*) H_2 (balloon), Pd/C, DMF-EtOH, 80°C, 80%; (*c*) HCTU, Et_3N, DMF, 0°C to RT, 24 h, 91%. For details, see the experimental section.

Table 1

Summary of binding data for compounds of the present study.

No.	Formula	Linker	R_1[a]	R_2[a]	CD40 IC_{50} [μM]	TNF IC_{50} [μM]	NF-κB IC_{50} [μM]	B cell IC_{50} [μM]
1	$C_{45}H_{32}N_{10}O_{21}S_6$				2.26		42.7	
5	$C_{24}H_{17}N_3O_7S$	benzene	1-SO_3H	4'-NO_2	341.6	>1000		
6	$C_{30}H_{21}N_3O_7S$	biphenyl	1-SO_3H	4'-NO_2	0.31	>1000	10.3	13.2
7	$C_{30}H_{21}N_3O_7S$	biphenyl	5-SO_3H	4'-NO_2	2.33	478.6		
8	$C_{30}H_{23}N_3O_5S$	biphenyl	1-SO_3H	4'-NH_2	301.0	886.9		
9	$C_{30}H_{21}N_5O_5S$	biphenyl	1-SO_3H	3',4'-(N=N-NH)-	0.99	>1000		
10	$C_{32}H_{24}N_2O_7S$	biphenyl	1-SO_3H	4'-CO_2Me	0.17	992.0	17.1	4.5
11	$C_{31}H_{21}N_3O_6$	biphenyl	5-CO_2H	4'-NO_2	0.36	>1000	9.4	15.9

[a]For numbering, see structure **6** in Scheme 1.